NTNU – Trondheim
Norwegian University of
Science and Technology

Modeling of Hybrid Marine Electric Propulsion Systems

Øyvind Rønneberg Gåsemyr

Marine Technology
Submission date: June 2014
Supervisor: Eilif Pedersen, IMT

Norwegian University of Science and Technology
Department of Marine Technology

Preface

The M.Sc. thesis is mandatory for all master students attending the Department of Marine Technology at NTNU in Trondheim. The thesis accounts for 100 % of the workload during the tenth semester and is equal to 30 ECTS.

The subject of the thesis was developed in collaboration with the Department of Marine Technology at NTNU in Trondheim and ABB Marine. The subject was adjusted to meet my background and interest as far as possible.

The thesis revolves around modeling and simulation of diesel-electric power systems utilizing energy storage devices in order to reduce load variations on the power plant, hence reducing emissions and increasing fuel efficiency.

I would like to thank Associate Professor at NTNU, Eilif Pedersen for guidance and assistance during the thesis work. I would also like to thank Børre Gundersen (R&D manager at ABB) and Kristoffer Dønnestad (R&D engineer at ABB) for providing technical assistance throughout the project.

Øyvind Rønneberg Gåsemyr, Trondheim 10.06.2014

Abstract

Energy storage devices integrated in diesel-electric power systems is believed to have potential also in marine applications. For certain load conditions energy storage can act as load buffers which will decrease the load variations on the generator sets, hence optimizing the operation when is comes to emissions and fuel efficiency.

In this context this thesis is aimed at development of simulation tools for hybrid marine electric propulsion systems. Assessment of two energy storage concepts is included, focusing on how their different attributes is utilized in the best manner. The bond graph language is chosen for modeling the physical components, because of its ability to represent the power interaction between a large selection of energy domains.

Component models of the essential electrical and mechanical components on the consumer side of a conventional diesel-electric propulsion system is modeled and connected. Additionally component models of a rechargeable battery and a supercapacitor is implemented to the model. A simple power control method is used to control the power flow of the energy storage devices .

Hybrid power plants are complex systems and the simulation tool developed in this thesis is considered far from complete, especially when it comes to control systems. To determine the actual reduction in fuel efficiency and emissions, dynamic models of diesel engines and generators should be added. However the model serves as a promising basis for further development. It visualizes the peak shaving effect from the power input point of view as expected and the principles of utilizing energy storage under varying load conditions.

Contents

List of Tables

List of Figures

Nomenclature

Abbrevations

AC	Alternating current
DC	Direct current
DP	Dynamic Positioning
DOD	Depth of discharge
EB	Electrochemical battery
ECA	Emission Control Area
EDLC	Electric double-layer capacitor
EPR	Equivalent parallel resistance
MCR	Maximum continuous rating
OSV	Offshore supply vessel
PMS	Power Management System
PSV	Platform Supply Vessel
SC	Supercapacitor
SOC	State of charge
SPJ	Switched power junction
VSI	Voltage Source Inverter

Uppercase

0	[-]	Bond graph 0-junction
1	[-]	Bond graph 1-junction
A	[V]	Amplitude of exponential zone
A_1, A_2, A_3	[-]	Sector decision variable
B	$[Ah^1]$	Inverse of exponential zone time constant
C	[-]	Bond graph capacitor element
Cs	[F]	Equivalent capacitance
E_0	[V]	Constant Battery Voltage
Ec	[J]	Energy capacity of a capacitor bank
GY	[-]	Bond graph gyrator
I	[-]	Bond graph inertia Element
Ib	[A]	Battery current
K	[V]	Polarization constant
L_s	[H]	Stator self-inductance
L_r	[H]	Rotor self-inductance
L_m	[H]	Mutual inductance
Q	[Ah]	Battery Capacity
R	[-]	Bond graph resistor element
Ri	[Ohm]	Internal Resistance
S_1, S_2, S_3	[-]	Inverter control variable
Se	[-]	Bond graph effort source
Sf	[-]	Bond graph flow source
TF	[-]	Bond graph transformer
T_p	[Nm]	Propeller load torque
V_s	[v]	Equivalent voltage
V_T	[V]	Terminal Battery Voltage

Lowercase

f	[Hz]	Frequency
i_a	[A]	Current in abc-frame
i_b	[A]	Current in abc-frame
i_c	[A]	Current in abc-frame
$i_{\alpha s}$	[A]	α-component of the stator current
$i_{\beta s}$	[A]	β-component of the stator current
$i_{\gamma s}$	[A]	γ-component of the stator current
i_{ds}	[A]	d-component of the stator current
i_{qs}	[A]	q-component of the stator current
i_{dr}	[A]	d-component of the rotor current
i_{qr}	[A]	q-component of the rotor current
m	[-]	Transformer modulus
n	[RPM]	Engine speed
p	[-]	Number of poles
r_s	[Ω]	Stator resistance
r_r	[Ω]	Rotor resistance
s	[-]	slip
$v_{\alpha s}$	[V]	Stator voltage in $\alpha\beta$-frame
$v_{\beta s}$	[V]	Stator voltage in $\alpha\beta$-frame
v_{ds}	[A]	d-component of the stator voltage
v_{qs}	[A]	q-component of the stator voltage
v_{dr}	[A]	d-component of the rotor voltage
v_{qr}	[A]	q-component of the rotor voltage
v_a	[V]	Voltage in abc-frame
v_b	[V]	Voltage in abc-frame
v_c	[V]	Voltage in abc-frame

Greek

ω_p	$[\frac{rad}{s}]$	Propeller speed
ω_r	$[\frac{rad}{s}]$	Rotor speed
ω_s	$[\frac{rad}{s}]$	Synchronous speed
ω_{slip}	$[\frac{rad}{s}]$	Slip speed
$\psi_{\alpha s}$	[V]	Stator flux component in $\alpha\beta$-frame
$\psi_{\beta s}$	[V]	Stator flux component in $\alpha\beta$-frame
ψ_s	[V]	Stator flux
ψ_{ds}	[V]	d component of the stator flux
ψ_{qs}	[V]	q component of the stator flux
ψ_{dr}	[V]	d component of the rotor flux
ψ_{qr}	[V]	q component of the rotor flux

Chapter 1

Introduction

1.1 Motivation

Transient operation of diesel engines, caused by quick load variations is a significant source for pollutant emissions. The effects of transient operation of diesel engines in marine applications have gained more attention in recent years. There is believed to be great benefits in analysis, modeling and simulations of both internal combustion engines and complete power systems. New solutions for control, optimization and simulation are needed for the emerging hybrid marine power plants.

1.2 Problem

The focus in this thesis has been on development of a simulation model of a hybrid marine electrical power system using the bond graph method. Hybrid systems utilizes energy storage to optimize the operation when is comes to fuel consumption and emissions. Component models of such energy storage devices is developed and implemented. For this thesis a supercapacitor and a rechargeable battery is chosen for energy storage. Modeling of hybrid power plants requires insight into several energy domains and engineering disciplines. Chemical energy trapped in the fuel is converted to thermal energy during combustion. Expansion of the trapped gases create a force on the piston, which generates mechanical torque on the engine shaft. Power is transformed from the mechanical domain to the electrical by connecting the engine shaft to a generator. And by use of advanced control systems and complex electrical components the desired propeller speed and torque is obtained. Flexible and accurate simulation models of multi-domain power plants are extremely useful and cost-effective compared to physical prototypes. On the other hand modeling of these multi-disciplinary systems requires a large amount of effort and knowledge.

To limit the workload in this thesis to an acceptable level, the simulation model is limited to consist of the components on the consumer side of the power plant, in

addition to the two energy storage devices. A simplified control unit for controlling the power flow of the energy storage devices is also developed and added to the model.

Both modeling and simulation has been carried out in the simulation and modeling software 20-sim.

1.2.1 Scope of work

- Investigate the emerging technologies in marine electric power systems and identify the main differences and advantages compared to conventional marine power systems.
- Identify the main benefits of energy storage devises in marine power systems.
- Perform a literature study on the concepts of energy storage and conversion, and the characteristics and principles of rechargeable batteries and supercapacitors.
- Development of energy storage models.
- Development of models of the components on the consumer side of a hybrid marine electrical power system.
- Carry out performance simulations of the battery and the supercapacitor and running two case simulations of the complete model.

1.3 Organization of the thesis

Chapter 2: Includes a brief introduction to conventional diesel-electric propulsion systems. New concepts and technologies which are applied and under development are also investigated.

Chapter 3: Presents a review of the main devices for energy storage and conversion, with emphasis on electrochemical batteries and supercapacitors.

Chapter 4: Presents the theoretical basis of the system components, along with a their bond graph representation. A brief introduction to the bond graph method is also included.

Chapter 5: Presents the simulation results of the two energy storage models and results from two case simulations.

Chapter 6: Conclusion and recommendations for further work.

Appendix A: Presents the parameter calculations of the induction motor.

Appendix B: Source code from 20-sim for various model elements and components.

Chapter 2

Diesel-electric propulsion systems

The use of electric propulsion is not a new idea, and the concept dates back to the 1920s when steam generators were used in transatlantic passenger lines. But the more efficient and economical diesel engine eventually replaced the steam generator in most applications. It was first when the AC motor drives was introduced in the 1980s the use of electrical propulsion emerged in new applications [1]. Today diesel-electric propulsion systems can be found in cruise ships, field support vessels, semi-submersible drilling rigs, etc. The introduction of azimuth thrusters and podded propulsion units during the 1990s highlighted various advantages of diesel-electric propulsion systems. [1] Summarizes the advantages of diesel-electric propulsion to the following:

- Electric power can be fed through cables to electric motors at any location in the vessel independent of the location of the prime mover. Thus increasing the maneuverability and the space utilization of the vessel.
- The prime movers are usually represented by medium speed diesel engines, which have a lower weight and lower investment costs than equally rated low speed engines used in direct mechanical propulsion.
- Noise and vibration levels are reduced as a result of prime movers running at constant speed, in addition to shorter shaft lines.
- The possibility to optimize the number of running generator sets to meet power demands at different operational profiles (dynamic positioning, maneuvering, transit, etc.), thus reducing fuel consumption and air emissions.
- Reduced maintenance, as a result of optimal operation of the prime movers.
- The possibility to separate the propulsion systems physically to increase reliability and to meet redundancy requirements.

- Electric propulsion systems can provide maximum torque also at low speeds, which is important for ice going vessels where the propeller can be jammed or blocked with ice.

2.1 Conventional system description

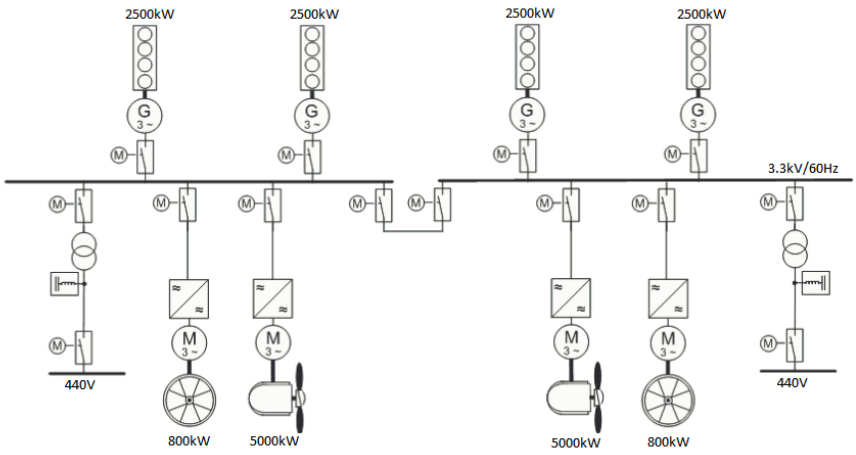

Figure 2.1: Conventional electric power and propulsion plant for a typical offshore support vessel [2].

Today a conventional diesel-electric propulsion systems consists of multiple prime movers (diesel engines, gas engines, steam turbines, etc.), which acts as the source of power. The generators produce AC current with a frequency proportional to the rotational speed of the prime mover. The AC current is distributed through the main switchboards to the different consumers on board the vessel. Transformers isolate the electric power distribution into several partitions with different voltage levels to meet the requirements of the consumers (thrusters, hotel loads, auxiliaries, etc.). For vessels with dynamic positioning (DP) systems, the switchboard is split in two, three or even four systems to meet redundancy requirements. The position keeping ability is then maintained, also upon worst case single failure of one section [1]. Electrical motors transform the electric power into mechanical power, which is to be used for propulsion, cranes, winches, pumps, etc. Today most propulsion units operate with fixed pitch, this means that the thrust only varies with the speed of the propeller. The propeller speed is controlled through variable speed drives which converts the frequency of the AC-current before it is supplied to the electric motor. The voltage source inverter (VSI) is by far the most used converter. The switching elements of the rectifier and inverter in the VSI are controlled to give the electric motor the desired speed [1]. The overall control of the power

system is performed by the power management system (PMS). The objective of the PMS is to ensure sufficient amount of available power for the actual operation mode. This is done by comparing the available power and the consumed power, and if needed, additional generators are started or stopped. By controlling and monitoring the energy flow, the power management system utilizes installed and running equipment to ensure optimal fuel efficiency [1].

2.2 Drivers for change

During the 1990s the increased attention to the effect air pollution had on global warming led to new regulations restricting the content of nitrogen oxides (NO_x), sulphur oxides (SO_x) and particulate matter (PM) in the exhaust gas from diesel engines. MARPOL Annex VI sets limits for NO_x emissions from diesel engines. The Tier levels refer to the maximum allowed NO_x emissions per kWh produced. Tier I applies for all engine installed after January 2000. Tier II takes effect on all engines installed after January 2011, and calls for a NO_x reduction of 16 - 22 % depending on the size of the engine. The Tier III standard will take effect as of January 2016, and calls for a reduction in NO_x emission of 80 % relative to Tier I, but its area of application restricted to Emission Control Areas (ECA). Areas which most likely will fall into this category are among others the North Seas, The Baltic Sea and North America [3].

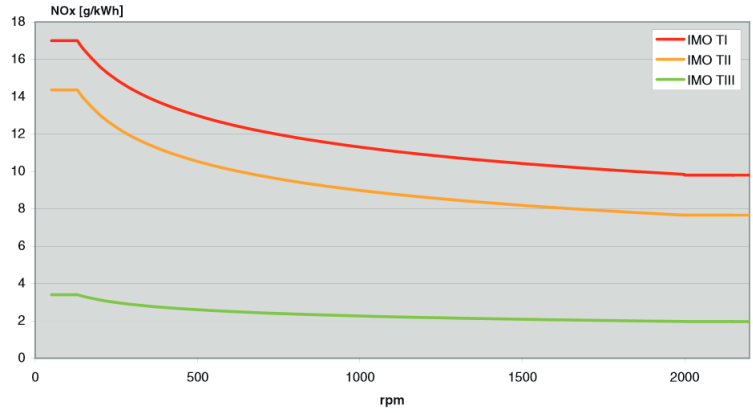

Figure 2.2: MARPOL Annex VI, (NO_x) emission limits [3].

The legislation is stringent and national penalties for non-compliance can be severe.

2.3 New technologies and future aspects

2.3.1 Fuels cells in marine applications

Fuel cell technology has recently proved to be successful in marine applications, as demonstrated by the Fellowship project. The joint industry project resulted in the installation of a 330 kW fuel cell in the offshore supply vessel Viking Lady, and has as of 2012 resulted for more than 7000 hours of smooth operation. Fuel cell technology builds on conversion of the chemical energy trapped in the fuel into electrical energy through electrochemical reactions. The process itself is quite similar to the process in electrochemical batteries, where reactions occur at the interface between the anode and cathode, though a continuous supply of air and fuel is required. Bi-products of the power generation from fuel cells are heat and H_2O. The main advantages of introducing fuels cells to marine applications are an increased chemical efficiency, reduced CO_2 emissions and reduced noise and vibration levels on board the vessel [4].

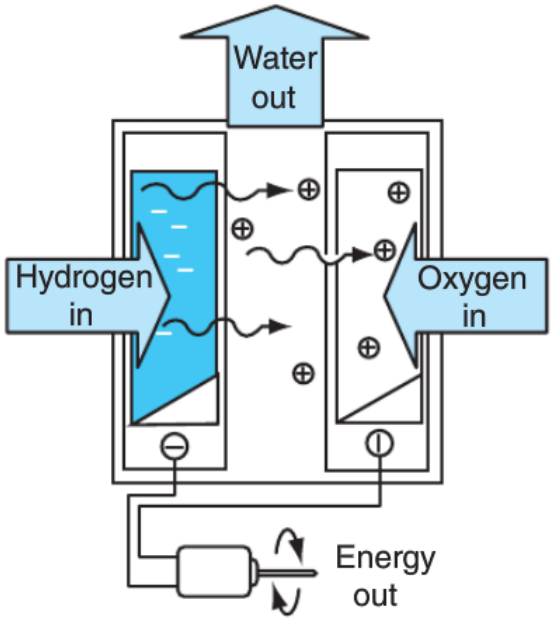

Figure 2.3: Basic principle of a fuel cell [5].

2.3.2 Propulsion systems using pure battery power

Lately there has been tremendous development in the energy storage technology, which enables vessels traveling short distances to utilize batteries as the only power source. An example is the ferry designed and built by Siemens in cooperation with Fjellstrand shipyard. The ferry which is operated by Norled AS runs on electric power supplied by rechargeable lithium-ion batteries alone. The batteries are recharged in 10 minutes each time the ferry docks to drop cars on and off, and are sized for crossing the fjords of western Norway. The ferry is designed optimally in terms of weight and hull shape, to reduce the energy consumption. The ferry which has a capacity of 120 cars and 360 passengers is granted to serve the route between Lavik and Opedal from 2015 to 2025. The ferry currently serving this route consumes 1 million liters of diesel each year, and emits 2680 metric tons of CO_2 and 37 tons of NO_x [6]. This enlightens the reduction of the environmental footprint such new technologies can bring.

2.3.3 Hybrid system development

A hybrid system combines the conventional diesel-electric power generation with energy storage devices, such as batteries, supercapacitors and fuel cells. As a result of new emission legislation, the focus on hybrid marine propulsion and power systems has increased. The concept of hybrid propulsion systems is especially applicable for vessels with:

- Frequent variations in load demand, mainly operating at low loads.
- High requirements to power flexibility.
- Prime movers with operational limitations.
- Operation in environmental sensitive areas.

The concept is especially suitable for vessels with long operating periods in DP. During DP, the vessel is imposed by varying wave and wind forces, which must be counteracted by the thrusters. For a vessel with a conventional diesel-electric power system this fluctuating power demand must be supplied by the diesel engines alone. This results in transient operation of the diesel engines during DP. The most notable feature of transient operation of diesel engines is the turbocharger lag. Turbocharger lag is a result of the slow engine response after a load increase. During the early cycles of a transient event, and until the sufficient air supply and torque has been build up, larger amounts of soot and NO_x are emitted, than compared with steady state operation [7]

2.3.4 The onboard DC Grid

Previously the efficiency of the diesel engines has been limited by the fact that generators are required to supply AC-voltage to the main switchboard at a specific frequency (usually 50 or 60 Hz). As a result, the diesel engines are forced to run at

constant speed, depending on the number of poles p in the generator. The relation between frequency f and engine speed n is given by

$$f = \frac{p \times n}{120} \tag{2.3.1}$$

The best fuel efficiency for constant speed diesel engines are usually obtained at 80-85 % MCR (Figure 2.4). At lower loads, the fuel efficiency increases significantly. To remove this efficiency limitation, ABB has developed the onboard DC Grid. The onboard DC Grid is in fact an expansion of the DC-link found in conventional variable speed drives. The main difference from a conventional AC system is that electric power is fed from the generator via a rectifier into a common DC bus [6]. From the DC bus all consumers are fed by their own inverter unit. Further converters for energy storage devices can also be added. Figure 2.5 presents a single line diagram of a diesel-electric power system using the onboard DC grid. The prime movers can now be controlled independent from each other, and efficient operation is possible over a larger load range. All consumers are fed by their own inverter unit. This way, the thruster transformers and AC-switchboards are no longer necessary, hence reducing the total weight and space requirements of the diesel-electric propulsion system. The system is especially suitable for offshore vessels with long periods in DP-operation, where the average power demand is low. The first vessel equipped with this system was the platform supply vessel Dina Star, which was delivered to its owner Myklebusthaug Offshore AS in March 2013.

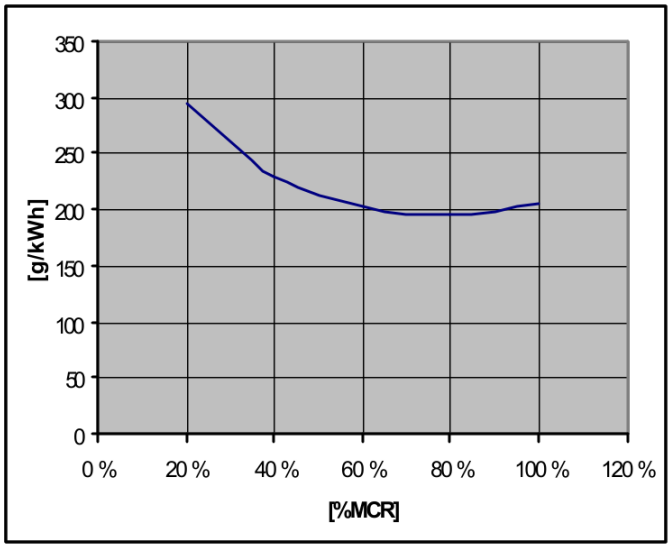

Figure 2.4: Typical fuel efficiency curve for diesel engines operating at constant speed [1].

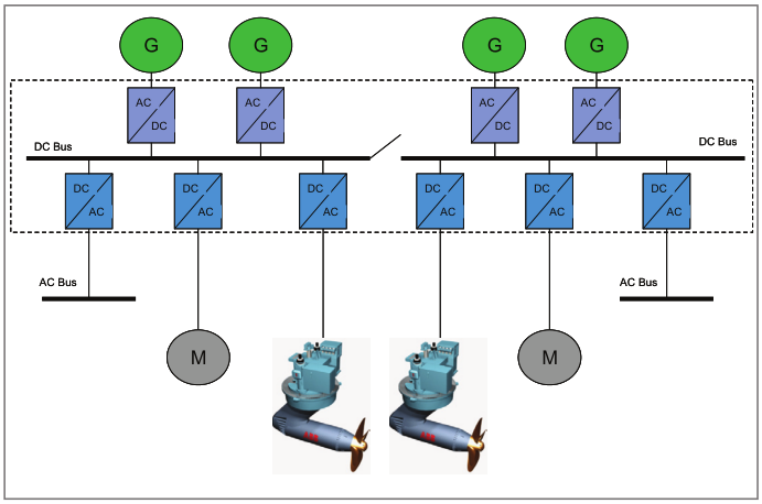

Figure 2.5: Single line diagram for a diesel-electric propulsion system with the Onboard DC grid installed[6].

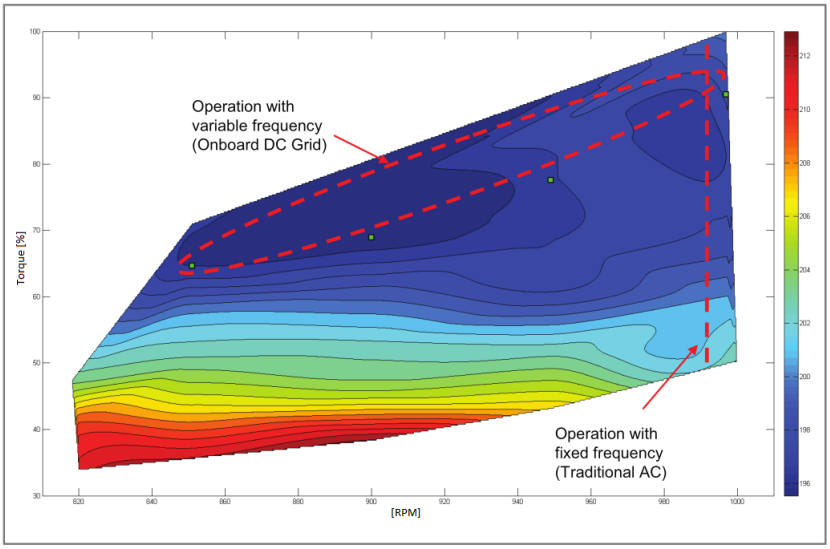

Figure 2.6: Fuel efficiency plot for diesel engines operating at variable speed [6].

[8] Summarizes the main benefits of the Onboard DC Grid to the following:

- Up to 20% reduction in fuel consumption, when utilizing all features including energy storage devices and variable speed operation of diesel engines.
- Reduced maintenance of engines by more efficient operation.
- Improved dynamic response by use of energy storage, which may result in better performance in DP operation, lower fuel consumption and more accurate station keeping.
- Increased payload of the vessel, due to lower space requirements and more flexible placement of electrical components.

Chapter 3

Energy storage devices

In todays world, clean energy technologies, which include energy storage and conversion, are becoming the most critical elements in overcoming fossil fuel exhaustion and global pollution. Of all the clean energy technologies, electrochemical technologies are considered the most feasible, environmental friendly and sustainable. With increasing demand in both energy and power densities of these electrochemical energy devices, further research and development are needed to overcome the challenges such as cost and durability, which are considered to be their major obstacles [9]. Figure 3.1 presents a Ragone plot of the different energy storage devices. A Ragone plot presents the power density of these devices along the ordinate versus their energy density along the abscissa. The supercapacitor have the ability to provide large amounts of power, but does not have the ability to store as large amounts of energy as a battery or a fuel cell. Choosing which energy storage device to use depends on the operational characteristics of the given system.

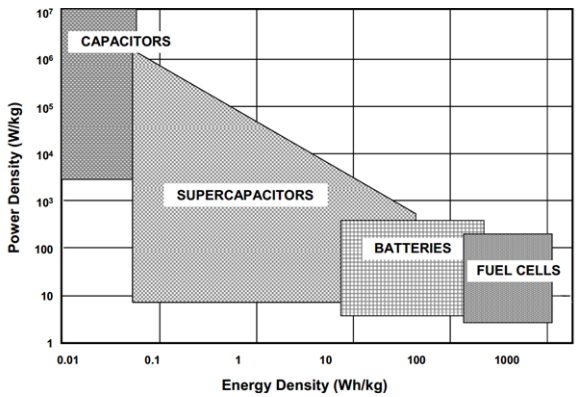

Figure 3.1: Ragone plot of different types of energy storage devices [10].

3.1 Electrochemical batteries

There are two types of batteries, primary and secondary:

Primary: The primary battery converts chemical energy into electrical energy by means of a non-reversible reaction. The main advantages of primary batteries are their low price and high energy density. The use of primary batteries is limited to applications where high energy density for one-time use is sufficient [12].

Secondary: Secondary batteries or the electrochemical rechargeable batteries are energy storage devices in which the electrochemical reaction is reversible. After discharge the battery can be recharged by injecting a direct current from an external source. In charge mode it converts the electrical energy into chemical energy. In discharge mode the reaction is reversed [12].

3.1.1 Cell behavior during charging and discharging

The cell has four essential components (figure 3.2). It interfaces to the external world through two metallic terminals. One connected to the negative electrode (anode), and one connected to the positive (cathode). During discharge, electrons pass from the anode to the cathode through an external load. To match the current of electrons in the circuit, ions in the cell flow towards the cathode [11]. When charging the cell, electrons are forced to move in the opposite direction by the external voltage. The ions in the cell flow towards the anode. This way the electrical energy is stored as chemical energy in cell [11].

To transport the ions between the anode and the cathode an electrolyte is used. An electrolyte traditionally is a aqueous solution with a high concentration of charged ions. The electrolyte comes in several different types, and depends on the intended application [11].

A separator is used to electrically isolate the positive and the negative electrode. Direct contact between the two electrodes will lead to short-circuiting, and discharging of the battery, making it useless. The separator allows closer spacing between the electrodes, thus reducing the total volume of the battery. The negative and positive electrodes are connected to an external terminal at the casing of the cell [11].

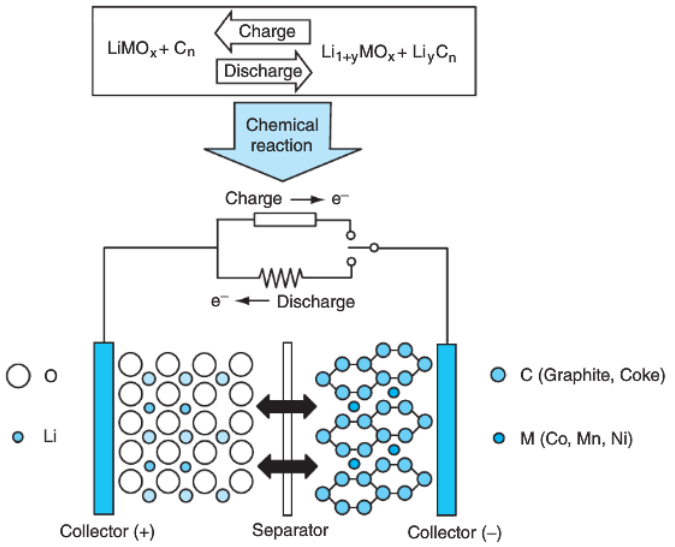

Figure 3.2: Essential components of a basic electrochemical cell [5].

3.1.2 Battery Terminology

Battery Voltage
The battery voltage varies with time and the level of charge. The term battery voltage refers to the average voltage during discharge [12].

Battery Capacity
The battery capacity represents the maximum amount of energy that can be extracted from the battery under certain conditions. The battery capacity is found by discharging the battery at a constant current until the voltage reaches a certain limit. The most commonly used measure for battery capacity is ampere-hours (Ah) [12].

Charge/discharge voltages
The measured terminal voltage of a cell will vary as it is charged and discharged. In an ideal battery there would be no difference between the charge and the discharge voltages. Both the charge and discharge curves have a plateau with little variation in voltage (figure 3.3). The average voltages in these plateaus are referred to as the charge and discharge voltages [12].

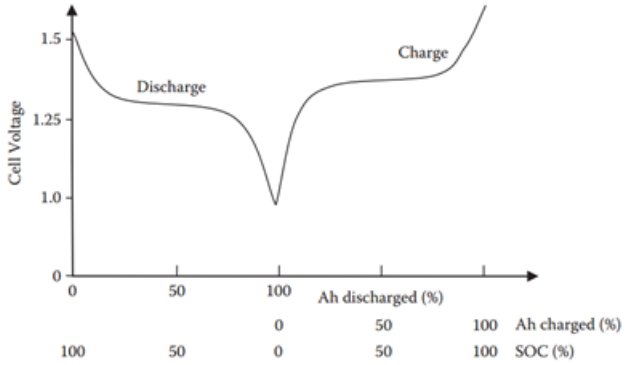

Figure 3.3: Discharge and charge curves of a 1.25 V cell [12].

The Coulombic efficiency
The coulombic efficiency is defined as the ratio between the amount of charge extracted from the battery during discharge and the amount of charge which enter the battery during charging. The value is always lower than unity [12].

$$\eta_{coulombic} = \frac{V_{discharge} \times Ah_{discharge}}{V_{charge} \times Ah_{charge}} \tag{3.1.1}$$

Self-discharge
Self-discharge occurs for all batteries, at a rate typically below 1 % per day, but there is some variation between different battery types. To avoid discharging at no-load conditions the battery can be trickle-charged at the same rate of the self-discharge [12].

State of charge
The state of charge (SOC) is defined as the ratio between the charge of the battery and the rated charge capacity. The depth of discharge (DOD), on the other hand is defined as the ratio between the charge drained from the battery and the rated charge capacity [12].

$$DOD = \frac{\int_0^t idt}{Q[Ah]} \cdot 100\% \tag{3.1.2}$$

$$SOC = \left(1 - \frac{\int_0^t idt}{Q[Ah]}\right) \cdot 100\% = 100\% - DOD \tag{3.1.3}$$

Memory effect
The memory effect is a phenomenon usually seen in nickel cadmium batteries, where the batteries remembers the C/D pattern and changes its performance accordingly.

The batteries gradually lose their charge capacity when being charged, after only being discharged partially [12].

3.1.3 Comparing different types of batteries

The cell stores electrochemical energy at low electrical potential typically from 1.2 to 3.6 V. This mainly depends on the electrochemistry of the materials involved [12].

In the current market there exist a large variety of batteries suited for different applications [9]. Parameters as price, charge capacity, cell voltage, durability, and energy density are important when choosing the battery for a given application. Figure 3.4 presents a Ragone plot of different types of batteries rated on their energy to weight ratio (Wh/kg) and their energy to volume ratio (Wh/liter). As we can see from the figure, the lithium-polymer batteries has the highest volumetric densities, but the use is limited as a result of a high initial cost.

The Li-ion batteries are the fastest growing battery type at the moment. It has a significantly higher volumetric energy density than many of its competitors. It also delivers a higher cell voltage, 3.5 V per cell [12]. The energy densities ranges from 100 [Wh/kg] to 200 [Wh/kg] for the best Li-ion batteries. Typical ratings in power density are between 1000 [W/kg] and 3000 [W/kg] [9].

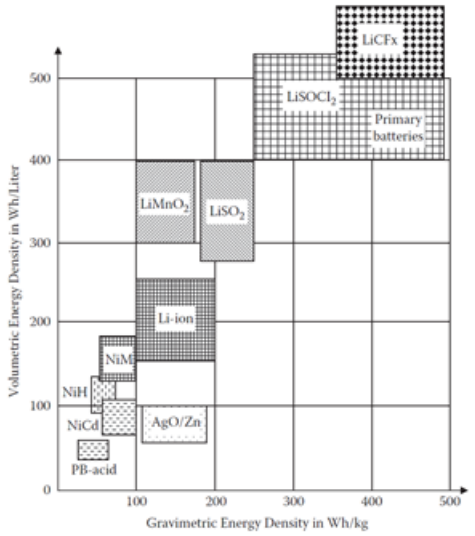

Figure 3.4: Ragone diagram for various electrochemical batteries [12]

3.1.4 Batteries and cells

A battery is made up of numerous electrochemical cells connected in series, parallel, or a combination. The required battery voltage and current for a given application determines how the cells are connected. A higher output voltage is obtained by increasing the number of cells connected in series, while a higher current is obtained by connecting more cells in a parallel configuration [12]. The battery capacity is raised by increasing the number cells.

3.2 Supercapacitors

The supercapacitor represents a relatively new type of energy storage device, even though the study of electrostatics and electrochemistry has been developed since the 17th century. Lately supercapacitors have received a significant level of interest for use in the electric utility industry for a variety of different applications [13]. Today use of supercapacitors is found in applications such as hybrid cars, buses and trains.

As a power device, the supercapacitor currently does not possess the high energy density compared to electrochemical batteries. On the other hand, they have a number of key attributes, such as the ability to charge and discharge within seconds, without any damage. This makes it possible to serve high power demands in short pulse intervals. Using a battery to serve such high power pulses will result in significant reduction of performance and life-time. Supercapacitors possess a near limitless recyclability with a typical life of more than 10^{6} cycles. Other advantages are environmental friendliness, low maintenance requirements, and safe operation over large temperature intervals [9].

3.2.1 Main types of supercapacitors

Supercapacitors are divided primarily by the charge mechanism and the materials used for electrode construction. There exist three general classifications of capacitors; electric double-layer capacitors, pseudo-capacitors, and hybrid capacitors. The electric double-layer capacitors stores energy electrostatically, the pseudo-capacitors stores energy electrochemically, while the hybrid capacitors uses a combination of the two mechanisms [9]. In this thesis, only the electric double-layer capacitors will be investigated further.

3.2.2 Electric double-layer Capacitors

The electric double-layer capacitors (EDLCs) are non-faradic systems. There is no transfer of charge between the electrolyte and the electrodes, in contrast to the electrochemical battery. As a result there are no chemical or compositional changes during charging and discharging. The lack of irreversible reactions between electrode and electrolyte results in a near limitless recyclability [9].

As explained the working principle of the EDLC involves no chemical reaction. The EDLCs consists of two electrodes, an electrolyte and two current collectors (figure 3.5). An insulating porous separator is placed between the two electrodes to avoid short-circuiting, but at the same time allow ion diffusion. When uncharged, the electrolyte consists of positive and negative ions, cations and anions. When charging the EDLC, the positive electrode attracts the anions, while the negative electrode attracts the cations [13]. The two layers of oppositely charged ions at the interphase between the electrode and the electrolyte give rise to the double layer capacitance in EDLCs [9].

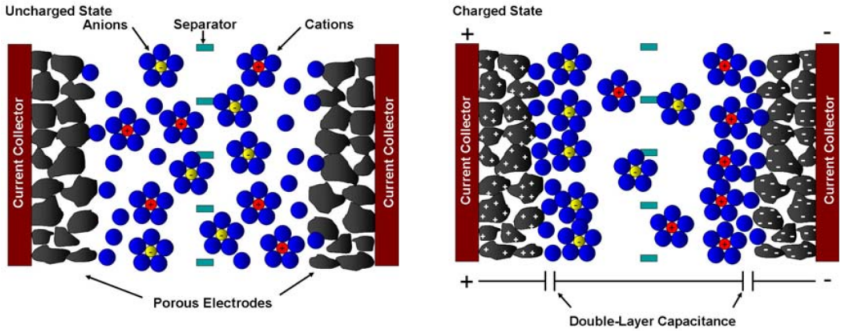

Figure 3.5: structure of electric double-layer capacitors [13].

Typical ratings for the EDLC in terms of power and energy density are 8000-10000 [W/kg] and 3-5 [Wh/kg] respectively [9].

3.2.3 Requirements for achieving higher performance

The rated voltage of the EDLCs is determined by the oxidation potential of the electrolyte. Electrolytes with oxidation potentials from 2.3 to 2.7 V per cell are common [13]. High surface area of the electrodes are important to develop the capacitive double layer. Activated carbon is the most commonly used electrode material, due to its low cost and high surface area [9].

3.2.4 Performance characteristics

The capacitance C, is defined as the ratio between the stored charge Q to the applied voltage V:

$$C = \frac{Q}{V} \tag{3.2.1}$$

An important performance value is the energy density of the supercapacitor. The energy density of a supercapacitor directly relates to the energy stored in each

supercapacitor cell. Assuming that the overall capacitance and voltage potential of the supercapacitor is known, the energy capacity of the supercapacitor is given by [9].

$$E = \frac{1}{2} C_s V_s^2 \tag{3.2.2}$$

To serve applications that require more power than a single supercapacitor can provide, it is necessary to stack cells. The overall capacitance and voltage potentials of series connected cells relate to the individual cell capacitance by:

$$\frac{1}{C_s} = \frac{1}{C_1} + \frac{1}{C_2} + ...\frac{1}{C_n} \rightarrow C_s = \frac{C_i}{n} \tag{3.2.3}$$

$$V_s = nV_i \tag{3.2.4}$$

Chapter 4

System Modeling

4.1 Bond graph modeling

The bond graph approach to modeling is based on identifying the energy flow in a physical system. The systems are broken down into ideal basic elements, and their interconnections are able to predict its behavior within reasonable accuracy. The lines between the elements represent the power flow between two ports and are called power bonds. A power bond transmits power instantaneously, with no loss. The direction of energy flow is indicated with a half arrow at the end of the power bond [20].

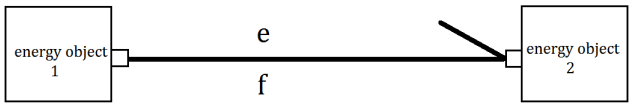

Figure 4.1: Power bond

There are two variables associated with each power bond, effort (e) and flow (f). These variables are known as power variables, and their product defines the power transmitted between these elements [20].

$$P(t) = e(t) \times f(t) \tag{4.1.1}$$

The energy transmitted in and out of the elements is the time integral of the power variable [20].

$$E(t) = \int_0^t P(t)dt \tag{4.1.2}$$

I addition to the power variables, the energy variables, momentum (p) and displacement (q) are useful to describe the energetic relation in a system [20]. The energy variables are defined as

Momentum:

$$p(t) = \int_0^t e(t)dt + p(0) \tag{4.1.3}$$

Displacement:

$$q(t) = \int_0^t f(t)dt + q(0) \tag{4.1.4}$$

These junctions can be viewed as energy switchboards, routing the energy into different paths. The first junction is the 0-junction. This junction defines a common effort on all the bonds connected to the junction. The 1-junction on the other hand, defines a common flow on all bonds connected to the junction.

There are 9 basic bond graph elements, which applies for energy storage, conversion, supply and dissipation. The table below presents the elements along with their constitutive relations [20].

Basic Element	**Mnemonic code**	**Constitutive relation**
Effort source	Se	*e=e(t)*
Flow source	Sf	*f=f(t)*
Capacitor element	C	*q=Ce*
Inertia Element	I	*p=If*
Resistor element	R	*e=Rf*
Transformer	TF	*e1=me2* *mf1=f2*
Gyrator	GY	*e1=f2r* *f1r=e2*
0-junction	0	*e1=e2=e3* *f1-f2-f3=0*
1-junction	1	*f1=f2=f3* *e1-e2-e3=0*

Table 4.1: Basic bond graph elements and their constitutive relations [20].

When modeling it is important to recognize which element to use when representing a given physical process. The bond graph method forms a powerful and useful tool for engineers to model dynamic systems in various energy domains.

4.2 Modeling of energy storage devices

4.2.1 The Lithium ion battery

There exists multiple mathematical models that describes the charge and discharge characteristic of a electrochemical battery. [14] Suggests a circuit-based model where the same equation is used both during charging and discharging. The model is a modified version of the equation developed by [**?**], which describes the electrochemical behavior of a battery directly in terms of terminal voltage, open circuit voltage, internal resistance, charging current and SOC [15]. The modified model uses only SOC as a state variable to describe the charge and discharge curves of the terminal battery voltage [14]. Figure 4.2 presents a typical discharge curve of a electrochemical battery. The terminal voltage is described by the following equation:

$$V_t = E_0 - R_i \times I_b - K\left(\frac{Q}{Q - \int_0^t idt}\right) + Ae^{(B \times ti)} \tag{4.2.1}$$

Where:

V_T	-	Terminal Battery Voltage [V]
E_0	-	Constant Battery Voltage [V]
Q	-	Battery Capacity [Ah]
R_i	-	Internal Resistance [Ohm]
$\int_0^t idt$	-	Actual battery charge [Ah]
A	-	Amplitude of exponential zone [V]
B	-	Inverse of exponential zone time constant [Ah^{-1}]
K	-	Polarization constant [V]

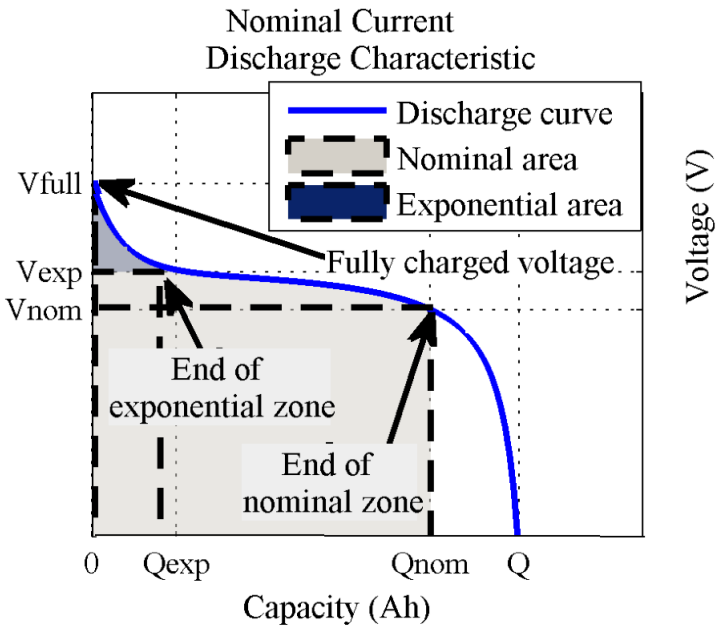

Figure 4.2: Discharge characteristics of a rechargeable battery [14].

The term $(Q/Q - \int_0^t idt)$ represent the non-linear change in voltage over time as the battery is discharged with the battery current. The exponential term $\mathrm{Ae}^{(-B\times it)}$ is represents the rapid voltage increase which occurs when the battery comes close to fully charged condition [14].

The model includes some assumptions and limitations. Temperature effects, self-discharge and the battery memory effect is not included. The internal resistance and the battery capacity are assumed to be constant, with no variations with the current amplitude. The model also assumes a coulombic efficiency of 100 %, which results in identical charge and discharge curves [14].

The main advantage of the model is the possibility to quite accurately represent the characteristics of several different electrochemical batteries, based on data commonly found in the manufacturers datasheet.

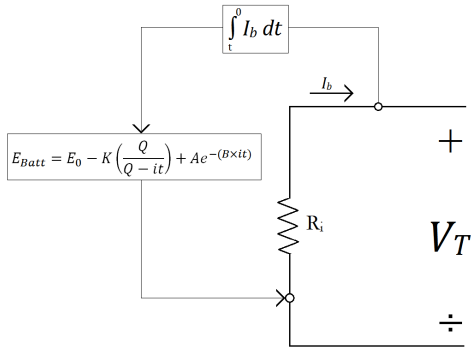

Figure 4.3: Mathematical battery model.

4.2.2 Bond graph representation of the rechargeable battery

There are several ways to model a rechargeable battery. In this thesis the model will be based on the mathematical representation described in chapter 4.2.

In electrical systems the power variables, flow and effort are represented by current and voltage respectively. The battery current which either charges or discharges the battery is modeled as a *Sf*-element. The internal resistance of the battery is modeled as a *R*-element. The battery voltage is set by a modulated effort source (*MSe*-element), which represents equation 4.2.1. To determine the amount of charge drained from the battery a displacement sensor is placed at the bond from the current source. The 1-junction accounts for the common current through the external load and the internal resistance, and a voltage drop over the internal resistance. The bond graph representation of the battery cell is presented in figure 4.4.

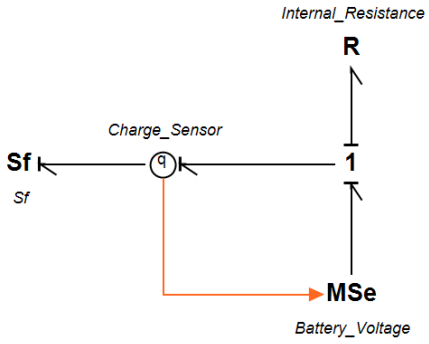

Figure 4.4: Bond graph representation of battery

4.2.3 Building a battery pack

By changing the parameters in the voltage equation, the model presented in figure 4.4 can be used both to represent a single cell and a complete battery bank consisting of multiple cells. There is still some interest in showing how a single cell model, can be used to develop models for battery banks. As previously explained the battery packs achieve their desired operating voltages by connecting cells in series. Cells connected in a parallel configuration increases the current capacity of the battery pack. A combination of parallel and series connected cells are used to achieve the performance requirements of the battery pack.

To model a battery pack we use the single cell model in figure 4.4 as a basis. In the battery pack model, each cell consists of the the *R*-element representing the internal cell resistance, and the *Mse*-element which represents the cell voltage source. In the the series branch the cells are connected by *1*-junctions, which represent the voltage difference over each cell. The same amount of current runs through all cells in each branch, so one charge sensor is sufficient for each branch.

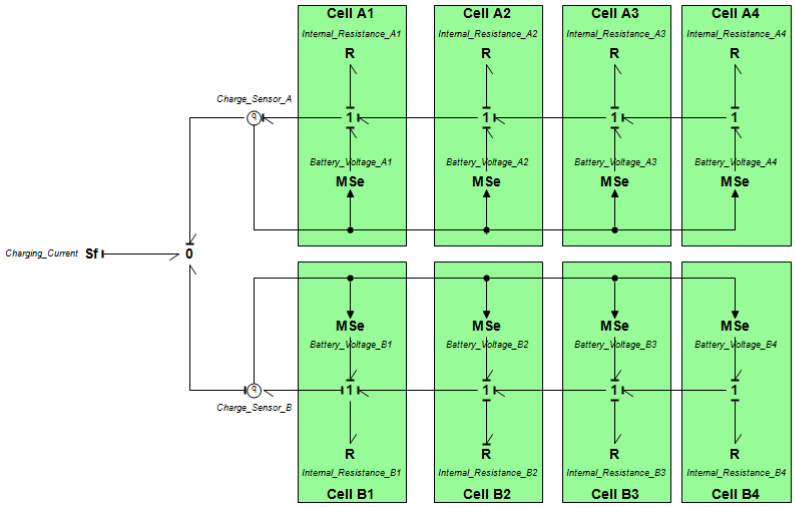

Figure 4.5: Bond graph representation of a battery pack.

4.3 The supercapacitor

A supercapacitor can easily be modeled by using some standard circuit elements. [16] Suggests the model presented in figure 4.6. The circuit model is for some products provided in the datasheet from the supercapacitor manufacturer EPCOS [17]. The advantage of this model is the easy determination of parameters, based on test results or manufacturer data.

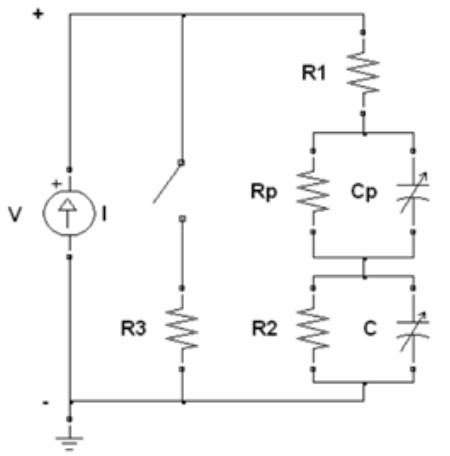

Figure 4.6: Basic conceptual model of a supercapacitor [18]

4.3.1 Parameter determination

Based on manufacturer data or experiment results the following steps should be carried out to calculate the necessary model parameters of the conceptual supercapacitor model.

During rapid change in charging current, the voltage level experiences an increased variation in the initial stage of the discharge process. When current suddenly passes through the resistor, the supercapacitor experiences an additional voltage drop, as illustrated in figure 4.7. By using the voltage drop in the initial stage of the discharging and the discharge current, the resistance of *R1* can be determined [16]. The resistance of *R1* is found by:

$$R_1 = \frac{\Delta V}{\Delta I} \tag{4.3.1}$$

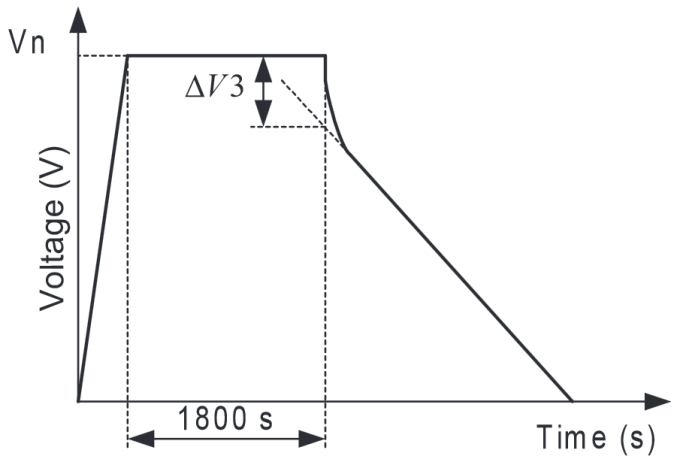

Figure 4.7: Typical voltage profile for charging and discharging of a supercapacitor [19]

The main capacitance of the supercapacitor is found by using the differences in charge and voltage between two points in the voltage curve. The charge is found as follows:

$$\Delta Q = \int_{t_0}^{t_1} i dt \tag{4.3.2}$$

Where i denotes the charging current. The main capacitance can then be found by

$$C = \frac{\Delta Q}{\Delta V} \tag{4.3.3}$$

or, if the energy capacity of the supercapacitor is known, the main capacitance can be found by

$$C = \frac{2Q}{V_2^2 - V_1^2} \tag{4.3.4}$$

The capacitance C_p represents the effect the voltage has on the total capacitance of the supercapacitor. [16] Suggests setting the value of C_p to be one thirteenth of C, which means that the element has a small impact on the supercapacitors performance.

$$C_p = \frac{C}{13} \tag{4.3.5}$$

In the same way as C_p, the purpose of the resistor R_p is to represent the effect the voltage has on the total capacitance of the supercapacitor. The resistance is best estimated by testing different values to find the one best matching experiment results. [16] Suggest setting this value to 10mΩ for a 350 F supercapacitor.

Self-discharge in supercapacitors is quite small which corresponds to a high resistance in *R2*. Again the resistance should be determined by testing different values to find the one best matching experiment results.

The main task for the resistor *R3* is to protect the supercapacitor from damages related to overcharging. A switch connects *R3* when the voltage reaches a certain level, and disconnects when the voltage has decreased to another. Given that the voltage limit has been reached, and that the resistor is connected, the resistance can be determined [16]. By looking at the voltage drop during in the period with no charging current, the resistance is given by:

$$R_3 = \frac{t_1 - t_0}{-ln(\frac{V_1}{V_2})C} \tag{4.3.6}$$

4.3.2 Bond graph representation of the supercapacitor

The modeling of the equivalent supercapacitor circuit starts with replacing all electrical elements with their bond graph equivalents. Converting an electrical network into a non-simplified bond graph is straightforward. Nodes in the circuit are replaced by 0-junctions. All elements and junctions are then connected according to the layout of the electrical circuit. Figure 4.8 presents the equivalent bond graph representation of the supercapacitor circuit model.

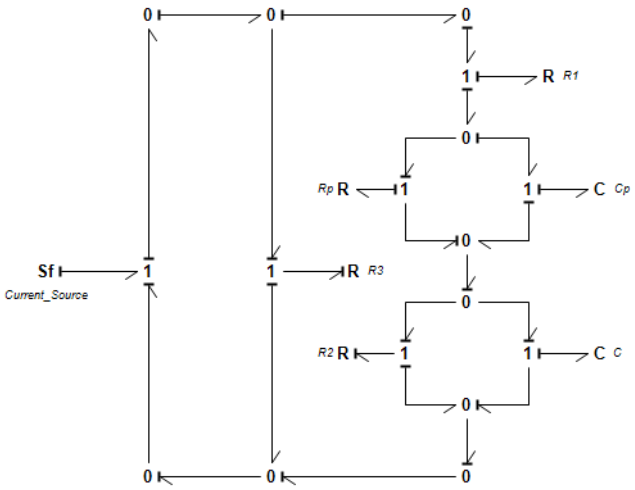

Figure 4.8: Non-simplified bond graph representation of the conceptual supercapacitor model.

By eliminating unnecessary junctions the bond graph can simplified to the one presented in figure 4.9. The simplified model does not present a direct symmetry with the circuit diagram, but it indicates the flow of power from the current source to the other elements in a good manner. Also included in the model is the switch which connects the resistor *R3*, when the voltage reaches a certain level.
Parameters of the various electrical components can now be implemented and the performance of the supercapacitor can be simulated.

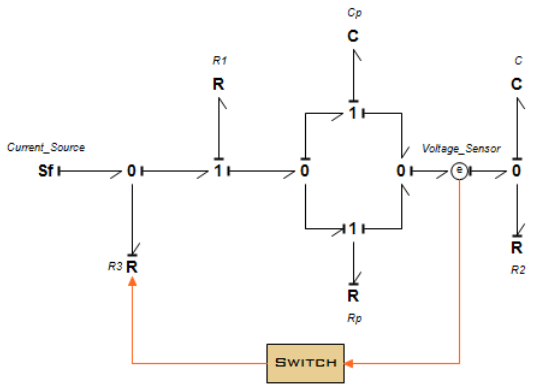

[H]

Figure 4.9: Simplified bond graph representation of the conceptual supercapacitor circuit.

4.4 The three-phase inverter

The inverter is the last part of the voltage source inverter. The desired frequency of the AC voltage is obtained by controlling the switching elements of the inverter. The three-phase inverter is build up of six switching elements which are turned on and off in a successive manner.

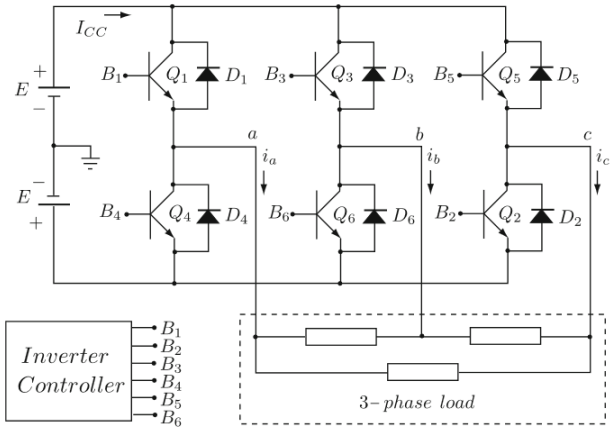

Figure 4.10: 3-phase transistor inverter [24].

Several methods can be used for controlling the switching of the inverter. In this thesis, motor control is based on Direct Torque Control (DTC) which will be reviewed in chapter 4.6. The bond graph modeling of the three-phase inverter starts

with introducing an expansion of the conventional 0- and 1-junctions. This is needed to model the ideal switching of the three identical half-bridges in the inverter [24].

4.4.1 Switched Power Junctions

[24] defines switched power junctions (SPJs) as *0*- and *1*-junctions which admits incoming effort (*0*-junction) or flow (*1*-junction) in more than one of their adjacent bonds. This will not imply a causal conflict because only one of these bonds is enabled at a given instant. The enabling and disabling of these bonds are performed by a set of control variables $U_1, U_2, U_3, ...U_n$. These variables take on the value of 1 or 0, where only one of the variables are allowed to have the value 1 at a given time instant. The symbols used to represent the SPJs are *0s* and *1s*. Figure 4.11 presents generalized *0s*- and *1s*-junctions.

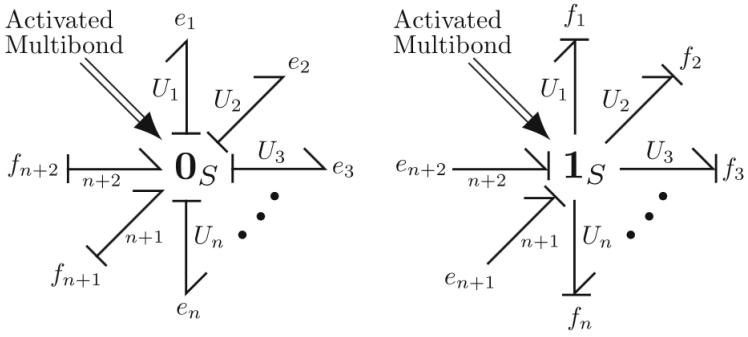

Figure 4.11: Generalized *0s*- and *1s*-junctions [24]

The constitutive relations of the SPJs presented in figure 4.11 can be written as

$$\text{Junction effort} = U_1e_1 + U_2e_2 + ... + U_ne_n \tag{4.4.1}$$

$$f_i = U_i(f_{n+1} + f_{n+2}); i = 1, ..., n \tag{4.4.2}$$

$$\text{Junction flow} = U_1f_1 + U_2f_2 + ... + U_nf_n \tag{4.4.3}$$

$$e_i = U_i(e_{n+1} + e_{n+2}); i = 1, ..., n \tag{4.4.4}$$

4.4.2 Bond Graph representation of the 3-phase inverter

The modeling of the inverter unit starts with assuming that each transistor-diode pair behaves like an ideal switch. The transistor-diode pairs are represented by *1s*-junctions. The *1s*-junctions model the switching the current through the transistor-diode pair between the line current $I_{a,b,c}$ (switch on) and 0 (switch off) [24]. The *0s*-junctions models the switching of the terminal voltage between $V_{dc}/2$ and $-V_{dc}/2$ which is supplied by the DC-link. The activated bonds supplies the SPJs with the control variables sent from the inverter control unit (*S1*,*S2* and *S3*). Figure 4.12 presents the complete bond graph representation of the three-phase inverter.

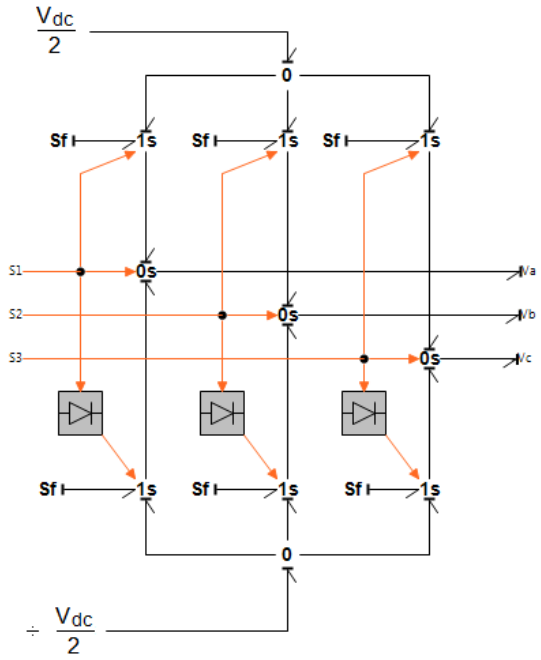

Figure 4.12: Bond graph representation of the inverter

4.5 The induction motor

The induction motor or the asynchronous motor is by far the most used motor to transform the energy from the electrical domain to the mechanical in diesel-electric propulsion systems. To simplify the modeling of the induction motor a coordinate transformation of the three-phase currents and voltages will be performed.

4.5.1 Operating principle

In the same way as for the synchronous motor, the asynchronous motor have a stator consisting of three-phase windings. The magnetic axes are shifted 120° relative to each other. The stator windings sets up a revolving magnetic field with a angular frequency determined by the network frequency. The speed of the revolving magnetic field is known as the synchronous speed, ω_s. In the asynchronous motor there is relative motion between the synchronous speed and the rotor speed, ω_r [25]. The relative speed difference is known as slip speed, and is given by:

$$\omega_{slip} = s\omega_s \tag{4.5.1}$$

Where the slip, s is defined as:

$$s = \frac{\omega_s - \omega_r}{\omega_s} \tag{4.5.2}$$

Slip increases with the loading of the induction motor. When slip exists a change of flux arises in the rotor. A electromotive force is induced, and a electrical current is established in the short circuited windings in the rotor. These short circuited windings are made up of aluminum bars formed as a squirrel cage, which in turn react with the magnetic field to produce a electromagnetic torque T_{em} [25].

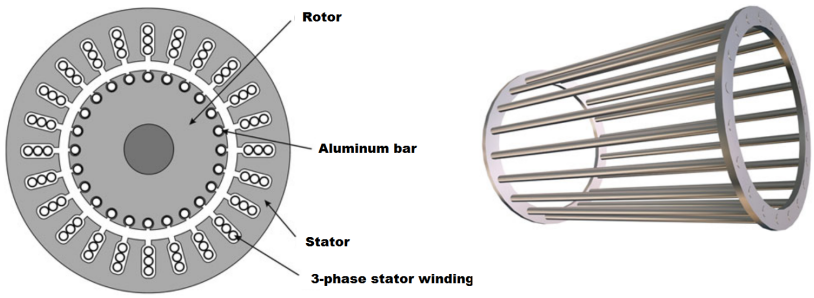

Figure 4.13: Crossection of the induction motor (left) and the squirrel cage (right) [25].

4.5.2 Power invariant transformation

The *dq*-transformation is a mathematical transformation used to simplify the analysis of both synchronous and asynchronous machines. The process of modeling the induction motor starts with performing a *dq*-transformation of the 3-phase current and voltage signals sent from the inverter unit. The three-phase alternating components in the *abc*-frame is defined in terms of the actual winding variables by applying the Park's transform [26]. The new variables are obtained by projecting the *abc*-components on three axes. The direct axis, the quadrate axis and the stationary axis [26].

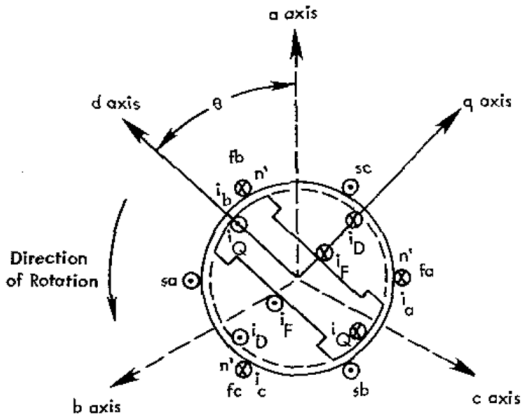

Figure 4.14: Projection of the *abc*-frame on the direct, quadrate and stationary axis [26].

4.5.3 Mathematical description of the power invariant transformation

The transformation from the *abc*-frame to the *dq*-frame is mathematically expressed as

$$\mathbf{i_{0dq}} = \mathbf{P} \cdot \mathbf{i_{abc}} \tag{4.5.3}$$

where the transformation matrix for the Park's transform $\mathbf{P}$ is given by

$$\mathbf{P} = \sqrt{\frac{2}{3}} \begin{bmatrix} \frac{1}{\sqrt{2}} & \frac{1}{\sqrt{2}} & \frac{1}{\sqrt{2}} \\ cos(\theta) & cos(\theta - \frac{2}{3}\pi) & cos(\theta + \frac{2}{3}\pi) \\ -sin(\theta) & -sin(\theta - \frac{2}{3}\pi) & -sin(\theta + \frac{2}{3}\pi) \end{bmatrix} \tag{4.5.4}$$

The inverse transformation is given by

$$\mathbf{i_{abc}} = \mathbf{P^{-1}} \cdot \mathbf{i_{0dq}} \tag{4.5.5}$$

$$\mathbf{P^{-1}} = \sqrt{\frac{2}{3}} \begin{bmatrix} \frac{1}{\sqrt{2}} & cos(\theta) & -sin(\theta) \\ \frac{1}{\sqrt{2}} & cos(\theta - \frac{2}{3}\pi) & -sin(\theta - \frac{2}{3}\pi) \\ \frac{1}{\sqrt{2}} & cos(\theta + \frac{2}{3}\pi) & -sin(\theta + \frac{2}{3}\pi) \end{bmatrix} \tag{4.5.6}$$

A criteria for the transformation is that the power before and after the transformation is identical. If this is true, the transformation is said to be power invariant. A transformation is power invariant if the transformation matrices are orthogonal [26]. This can be confirmed by the expressions above, because $\mathbf{P^T} = \mathbf{P^{-1}}$. As a result the power before and after the transformation should be identical.

$$P_{abc} \quad = v_a i_a + v_b i_b + v_c i_c = \mathbf{i_{abc}} \cdot \mathbf{v_{abc}^T}$$

$$= \left(\mathbf{P^{-1}} \begin{bmatrix} v_0 \\ v_d \\ v_q \end{bmatrix} \right)^T \left(\mathbf{P^{-1}} \begin{bmatrix} i_0 \\ i_d \\ i_q \end{bmatrix} \right) = \begin{bmatrix} v_0 & v_d & v_q \end{bmatrix} (\mathbf{P^{-1}})^\mathbf{T} \mathbf{P^{-1}} \begin{bmatrix} i_0 \\ i_d \\ i_q \end{bmatrix}$$

$$= v_0 i_0 + v_d i_d + v_q i_q = P_{0dq} \tag{4.5.7}$$

Easier filtering and control, is one of the main advantages of performing the dq-transformation. I addition the active and reactive power can be controlled independently by controlling the dq-components.

4.5.4 Bond graph representation of the *dq*-transformation

The bond graph representation of the power invariant dq-transformation is modeled as suggested by [21]. This model will be used between the inverter model and the model of the induction motor. The models input is the three-phase abc-voltages in addition to the position angle of the rotor in the induction motor θ. The output from the model is the dq-voltages. The causal strokes are assigned in such a way. Six modulated TF-elements are used to represent the multiplication of the transformation matrix. θ is used to determine the transformer modulus for all of the modulated TF-elements.

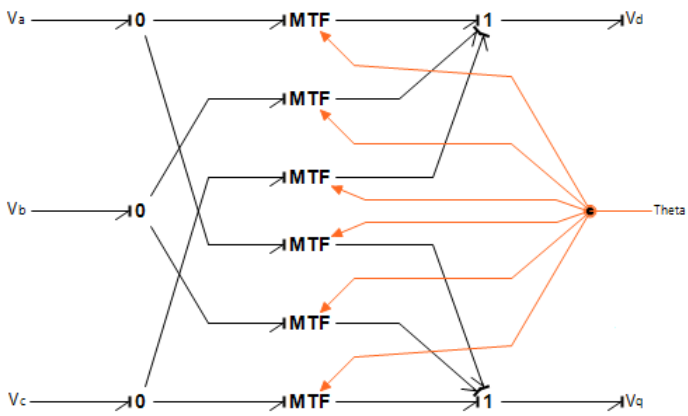

Figure 4.15: Bond graph representation if the Park's transformation from the *abc*-frame to the *dq*-frame.

4.5.5 Mathematical model of the induction motor

The voltage balance for the asynchronous motor is given by the following expression [21]:

$$\mathbf{v} = \mathbf{R}\mathbf{i} + \frac{d\boldsymbol{\psi}}{dt} \tag{4.5.8}$$

Using dq-components the voltages, currents, resistances and flux linkages are given by:

$$\mathbf{v} = \begin{bmatrix} v_{ds} & v_{qs} & v_{dr} & v_{qr} \end{bmatrix}^T \tag{4.5.9}$$

$$\mathbf{i} = \begin{bmatrix} i_{ds} & i_{qs} & i_{dr} & i_{qr} \end{bmatrix}^T \tag{4.5.10}$$

$$\mathbf{R} = \begin{bmatrix} r_s & 0 & 0 & 0 \\ 0 & r_s & 0 & 0 \\ 0 & 0 & r_r & 0 \\ 0 & 0 & 0 & r_r \end{bmatrix} \tag{4.5.11}$$

$$\boldsymbol{\psi} = \begin{bmatrix} \psi_{ds} & \psi_{qs} & \psi_{dr} & \psi_{qr} \end{bmatrix}^T \tag{4.5.12}$$

The flux linkages are related to the inductance matrix and the dq-currents by:

$$\boldsymbol{\psi} = \mathbf{L}\mathbf{i} \tag{4.5.13}$$

$$\begin{bmatrix} \psi_{ds} \\ \psi_{qs} \\ \psi_{dr} \\ \psi_{qr} \end{bmatrix} = \begin{bmatrix} L_s & 0 & L_m & 0 \\ 0 & L_s & 0 & L_m \\ L_m & 0 & L_r & 0 \\ 0 & L_m & 0 & L_r \end{bmatrix} \begin{bmatrix} \mathrm{i}_{ds} \\ \mathrm{i}_{qs} \\ \mathrm{i}_{dr} \\ \mathrm{i}_{qr} \end{bmatrix} \tag{4.5.14}$$

The rotor and stator current can be found by:

$$\mathbf{i} = \mathbf{L}^{-1}\boldsymbol{\psi} \tag{4.5.15}$$

The expressions for stator and rotor current then becomes [21]:

$$i_{ds} = \frac{-(-L_r\psi_{ds} + L_m\psi_{dr})}{L_sL_r - L_m^2} \tag{4.5.16}$$

$$i_{qs} = \frac{-(-L_r\psi_{qs} + L_m\psi_{qr})}{L_sL_r - L_m^2} \tag{4.5.17}$$

$$i_{dr} = \frac{L_s\psi_{dr} - L_m\psi_{ds}}{L_sL_r - L_m^2} \tag{4.5.18}$$

$$i_{qr} = \frac{L_s\psi_{qr} - L_m\psi_{qs}}{L_sL_r - L_m^2} \tag{4.5.19}$$

The expressions for the stator voltages, the rotor voltages and the electromechanical torque depends on weather we let the dq-reference frame rotate with the electrical rotor angular velocity (ω_r) or synchronous speed (ω_s) [21]. Letting the reference frame rotate at electrical rotor angular velocity ω_r, the voltage expressions are given as:

$$u_{ds} = r_s i_{ds} - \omega_r\psi_{qs} + \dot{\psi_{ds}} \tag{4.5.20}$$

$$u_{qs} = r_s i_{qs} - \omega_r\psi_{ds} + \dot{\psi_{qs}} \tag{4.5.21}$$

$$0 = r_r i_{dr} + \dot{\psi_{dr}} \tag{4.5.22}$$

$$0 = r_r i_{qr} + \dot{\psi_{qr}} \tag{4.5.23}$$

The electromechanical torque is expressed by:

$$T_e = \psi_{ds} i_{qs} - \psi_{qs} i_{ds} \tag{4.5.24}$$

The mechanical angular velocity of the rotor (ω_m) is related to the electrical angular velocity of the rotor (ω_r) by the number of pole pairs, p.

$$\omega_m = \frac{\omega_r}{p} \tag{4.5.25}$$

4.5.6 Bond graph representation of the induction motor

The bond graph representation of the induction motor is proposed in [21], and is based on the mathematical relations presented in chapter 4.5.5. The two *1*-junctions in the upper part of the model represents equation 4.5.20 and 4.5.21. The transformer represents equation 4.5.25. Stator and rotor resistances are represented by R-elements and the I-fields represents equation

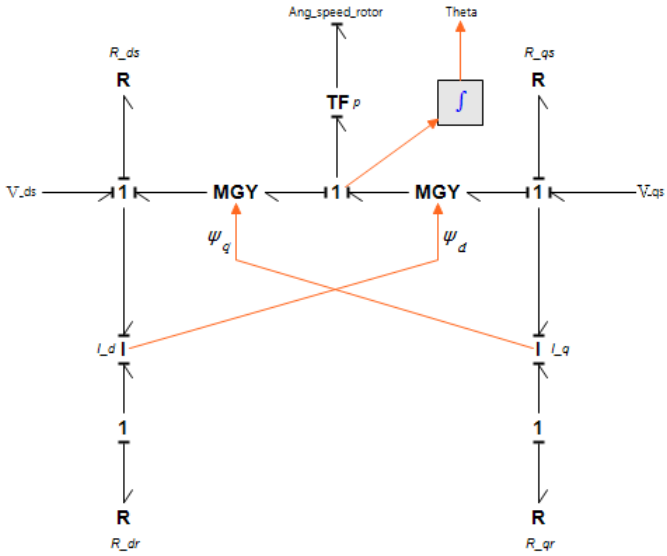

Figure 4.16: Bond graph model of the induction motor in the dq-frame letting the reference frame rotate with angular velocity, ω_r.

4.6 Direct Torque Control

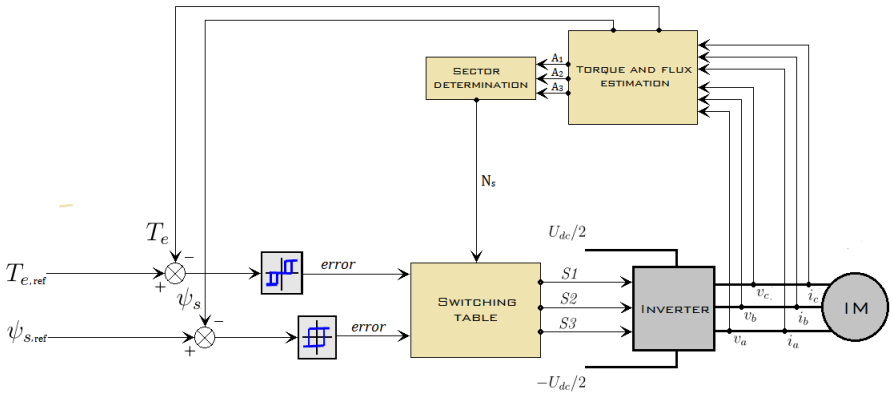

Figure 4.17: Control scheme using DTC for induction motor control

The control of the switching elements of the inverter unit is performed using Direct Torque Control (DTC). The inverter switches are regulated to achieve the required stator flux and motor torque. Optimal switching is done according to an predefined switching table. The electromagnetic torque (T_e) and the stator flux (ψ_s) is calculated using measurements from the three-phase currents and voltages which are fed into the induction motor. To simplify the calculations it is convenient to perform a Clarke coordinate transform of the voltage and current measurements from the *abc*-frame to the $\alpha\beta\gamma$- frame. The power invariant Clarke transformation matrix is expressed as [25]:

$$\mathbf{T} = \sqrt{\frac{2}{3}} \begin{bmatrix} 1 & -\frac{1}{2} & -\frac{1}{2} \\ 0 & \frac{\sqrt{3}}{2} & -\frac{\sqrt{3}}{2} \\ \frac{1}{\sqrt{2}} & \frac{1}{\sqrt{2}} & \frac{1}{\sqrt{2}} \end{bmatrix} \tag{4.6.1}$$

The matrix is used to transform both the voltages and the currents. The voltages in the $\alpha\beta\gamma$- frame are given by:

$$\mathbf{v}_{\alpha\beta\gamma} = \mathbf{T} \cdot \mathbf{v}_{\mathbf{abc}} \tag{4.6.2}$$

$$v_{\alpha s} = \sqrt{\frac{2}{3}}(v_a - v_b) + \frac{1}{\sqrt{6}}(v_b - v_c) \tag{4.6.3}$$

$$v_{\beta s} = \frac{1}{\sqrt{2}}(v_b - v_c) \tag{4.6.4}$$

$$v_{\gamma s} = 0 \tag{4.6.5}$$

The currents in the $\alpha\beta\gamma$- frame is given by:

$$\mathbf{i}_{\alpha\beta\gamma} = \mathbf{T} \cdot \mathbf{i}_{\mathbf{abc}} \tag{4.6.6}$$

$$i_{\alpha s} = \sqrt{\frac{2}{3}}(i_a - \frac{1}{2}i_b - \frac{1}{2}i_c) \tag{4.6.7}$$

$$i_{\beta s} = \frac{1}{\sqrt{2}}(i_b - i_c) \tag{4.6.8}$$

$$i_{\gamma s} = 0 \tag{4.6.9}$$

The stator flux components given by

$$\psi_{\alpha s} = \int (v_{\alpha s} - R_s i_{\alpha s})dt \tag{4.6.10}$$

$$\psi_{\beta s} = \int (v_{\beta s} - R_s i_{\beta s})dt \tag{4.6.11}$$

The magnitude of the stator flux is then determined by

$$\psi_s = \sqrt{\psi_{\alpha s}^2 + \psi_{\beta s}^2} \tag{4.6.12}$$

The electromagnetic torque T_e is estimated by [21]:

$$T_e = P(\psi_{\alpha s} i_{\beta s} - \psi_{\beta s} i_{\alpha s}) \tag{4.6.13}$$

Where P is the number of poles pairs in the induction motor.

There are three variables used as input for the switching table. d_T is found by comparing the estimated electromagnetic torque with the reference torque T_{ref}. $d_T = 1$ calls for an increase in torque, $d_T = 0$ indicates that the current torque should me maintained, while $d_T = -1$ calls for a decrease in torque. d_ψ is found by comparing the estimated stator flux with the reference value ψ_{ref}. $d_\psi = 1$ means that an increase of stator flux is needed, while $d_\psi = 0$ means that a decrease in stator flux is needed [23].

The last input variable needed for performing optimal operation of the inverter switches is N_s. It denotes in which sector the stator flux vector is located according to the six active voltage vectors and two null vectors presented in figure 4.18.

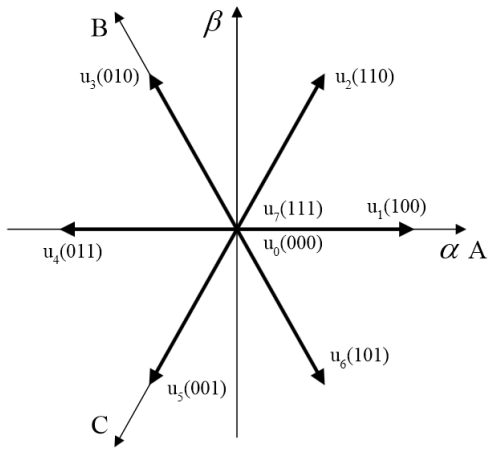

Figure 4.18: Voltage vectors [23]

The correct stator flux sector depends on the angle of the stator flux. The sector can be determined by using table 3.

A2	*A1*	*A0*	N_s
0	0	0	4
0	0	1	5
0	1	0	1
0	1	1	6
1	0	0	4
1	0	1	3
1	1	0	1
1	1	1	2

Table 4.2: Sector determination table [22]

The values *A1*, *A2* and *A3* is found by using the stator flux components calculated in equation 4.6.10 and 4.6.11. The following expressions are used [21]:

$$A_0 = \begin{cases} 1 & ,|\psi_{\beta s}/\psi_{\alpha s}| \geq 1/\sqrt{3} \\ 0 & ,|\psi_{\beta s}/\psi_{\alpha s}| < 1/\sqrt{3} \end{cases}$$

$$A_1 = \begin{cases} 1 & ,\psi_{\alpha s} > 0 \\ 0 & ,\psi_{\alpha s} \leq 0 \end{cases}$$

$$A_2 = \begin{cases} 1 & ,\psi_{\beta s} > 0 \\ 0 & ,\psi_{\beta s} \leq 0 \end{cases}$$

The correct signals which is to be sent to the six inverter switches can now be found by using the predefined switching table. Each vector u_1-u_8 contains the three switching signals S1, S2, S3.

d_ψ	d_T	N_s 1	2	3	4	5	6
1	1	u_2(1,1,0)	u_3(0,1,0)	u_4(0,1,1)	u_5(0,0,1)	u_6(1,0,1)	u_1(1,0,0)
1	0	u_7(1,1,1)	u_0(0,0,0)	u_7(1,1,1)	u_0(0,0,0)	u_2(1,1,1)	u_0(0,0,0)
1	-1	u_6(1,0,1)	u_1(1,0,0)	u_2(1,1,0)	u_3(0,1,0)	u_4(0,1,1)	u_5(0,0,1)
0	1	u_3(0,1,0)	u_4(0,1,1)	u_5(0,0,1)	u_6(1,0,1)	u_1(1,0,0)	u_2(1,1,0)
0	0	u_0(0,0,0)	u_2(1,1,1)	u_0(0,0,0)	u_2(1,1,1)	u_0(0,0,0)	u_7(1,1,1)
0	-1	u_5(0,0,1)	u_6(1,0,1)	u_1(1,0,0)	u_2(1,1,0)	u_3(0,1,0)	u_4(0,1,1)

Table 4.3: Predefined switching table [22]

The signals *S1*, *S2* and *S3* controls the on and off switching of the two switches in each of the three identical half-bridges. In example if $S1 = 1$ switch 1 is on, while switch 4 is off.

4.7 DC-DC Converter

The battery and the supercapacitor is connected between the positive and the negative side of the DC-link. The DC-link voltage is required to stay constant, which results in the need of a DC-DC converter. The DC-DC converter ensures that the output voltage from the energy storage devices matches the voltage level of the DC-bus. Though DC-DC converters in reality are controllable electrical circuits, the DC-DC converter is simply modeled as a MTF-element. The transformer modulus is expressed as

$$m = \frac{V_T}{V_{DC}} \tag{4.7.1}$$

4.8 The propeller

The propeller has the inertia J_p and is loaded by the torque T_p. The inertia is represented by an I-element. In the model, a single I-element accounts for the propeller inertia, the rotor inertia and the inertia of the propeller shaft. The load torque T_p is represented by an R-element and is typically expressed by

$$T_p = K * \omega_p^2 \tag{4.8.1}$$

where K is a constant, and ω_p represents the propeller speed.

A simplified representation of wave disturbances can easily be added to the model by adding a time dependent sinusoidal term. Thus the new expression for the load torque is given by

$$T_p = K \cdot \omega_p^2 (1 + A \cdot sin\left(\frac{2\pi t}{T}\right)) \tag{4.8.2}$$

where A determines the amplitude if the sinusoidal term and T is the wave period.

4.9 Power flow control

The power flow of the system is said to follow the law of energy conservation. The power consumed by the load should be equal to the power supplied by the power sources. The relationship between the power generated by the source (P_{source}), the power consumed by the load (P_{load}), and the power flow from the energy storage devices (P_{ESD}) is expressed as

$$P_{source} = P_{load} + P_{ESD} \tag{4.9.1}$$

where

$$P_{ESD} = P_B + P_{SC} \tag{4.9.2}$$

The expression above is used to calculate the charging current of the energy storage devices (ESDs). The ESDs can act as a load, as well as a source of power, depending on the direction of the power flow. To determine when to charge and discharge the ESDs, it is necessary to determine a limit for the power which should supplied by the generator, $P_{G,lim}$. Should the power demand of the load be higher than $P_{G,lim}$, the ESDs will deliver power in combination with the generator. Should the power demand from the load be lower than $P_{G,lim}$, power from the generator can be used to charge the ESDs. This way the load demand fluctuations seen by the generator is reduced. $P_{G,lim}$ should be set to the operating point where the fuel efficiency of the diesel engine is at its maximum. If the ESDs both become discharged, the power limitation should be ignored and additional generators should be connected to the power grid if necessary.

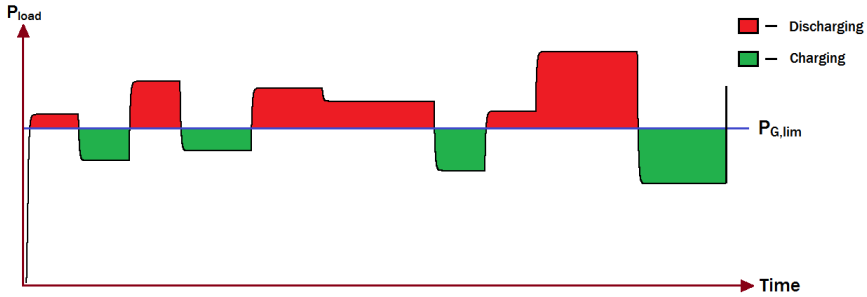

Figure 4.19: Charging and discharging during load variations.

The direction and amount of current flowing between the ESDs and the DC-grid is determined by

$$I_{ESD} = \frac{P_{source} - P_{load}}{V_{DC}} \tag{4.9.3}$$

In the model the desired charging current is obtained by controlling the resistance in a R-element. The resistance of the R-elements is given by

$$R_{ESD} = \frac{V_{DC}}{I_{ESD}} \tag{4.9.4}$$

4.9.1 SOC and voltage limitations

To ensure safe operation of the ESDs some limitations are defined in the proposed energy management system. The first limitation to consider is the state of charge (SOC). The terminal voltage (V_T) of the battery will decrease during discharge. This will increase the current drawn from the battery to provide a constant power output. As a result the system rating will increase and there is a risk of overheating the battery. Discharging the battery to low SOC values are also not recommended due to the related shortening of its cycle life. Lower limits for the value of SOC is therefore required. As the upper limit for the value of SOC is 100%, overcharging the battery will not be possible.

The maximum supercapacitor voltage is equal to the DC-voltage of the network.

4.10 The complete power plant

To investigate the behavior of the power plant all the component must be connected. Two *Se*-elements will be used to represent DC-bus voltages $V_{dc}/2$ and $V_{dc}/2$. The *Se*-elements will serve as the power input to the system. The model for the complete power plant is presented in figure 4.20.

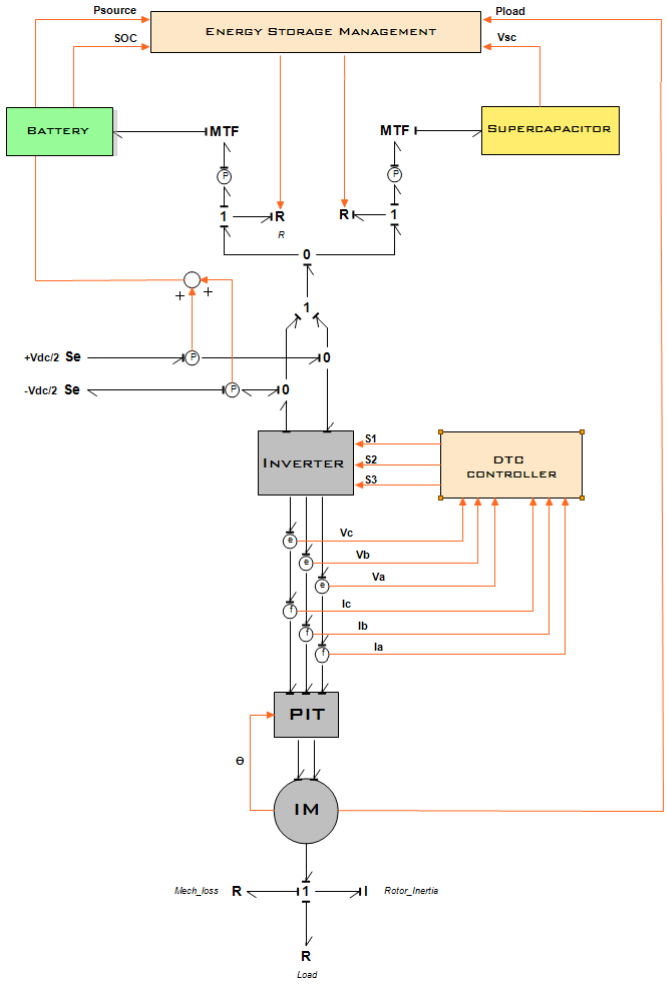

Figure 4.20: Complete system model.

Chapter 5

Results

Before the simulations can be carried out several parameters needs to be specified. The induction motor chosen for the simulations has a rated power output of 200 [kW], which will serve as a basis when assuming the rest of the model parameters. The procedure for determining the induction motor parameters can be found in appendix A, along with the values used in the model. Key model parameters will be specified with their corresponding simulation plots, while the remaining parameters can be found in appendix B along with the source code from 20-sim.

5.1 Simulation energy storage performance

5.1.1 The battery pack

The battery is assumed to possess a charge capacity of 79.5 [Ah], a energy capacity of 7.6 [kWh] and a average battery voltage of 96 V. The parameter values are set to manipulate a typical discharge curve of a Li-ion battery. Table 5.1 presents all model parameters and their assumed values.

Parameter	**Sign**	**Value**
Battery constant voltage	E0	96 V
Battery Capacity	Q	79.5 [Ah]
Polarization constant	K	3.5 [V]
Amplitude of exponential zone	A	7[V]
Inverse of exponential zone time constant	B	0.0002[Ah^{-1}]
Internal resistance	Ri	0.01[Ω]

Table 5.1: Model parameters for the battery model

Figure 5.1 presents the simulation results of a complete discharge of the lithium-ion battery. The discharge current is set to 100 [A].

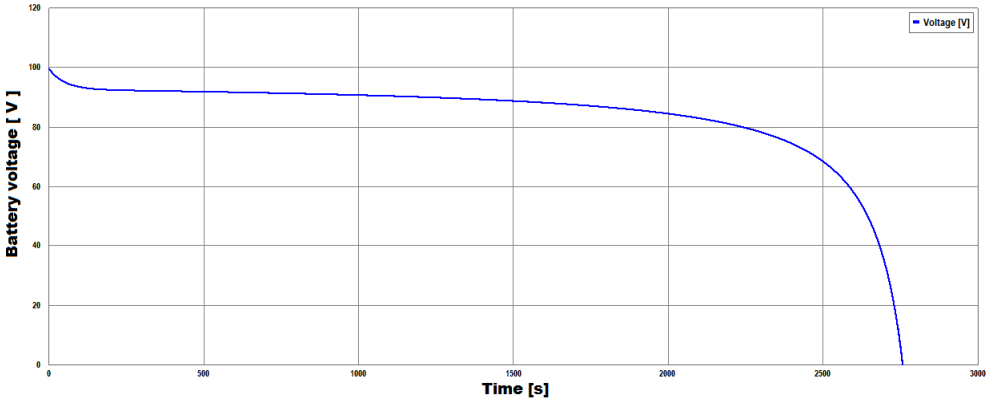

Figure 5.1: Discharge curve of the battery, $I_b = -100[A]$.

5.1.2 Supercapacitor

The model parameters of the supercapacitor is determined by first assuming that its energy capacity is 5% percent of battery energy capacity. The maximum allowed supercapacitor voltage is chosen to be the same as the bus voltage. The main capacitance is then found by equation 4.3.4. All model parameters are given in table 5.2. The resistance R

Component	$R_1[\Omega]$	$R_2[\Omega]$	$R_3[\Omega]$	$R_p[\Omega]$	C[F]	$C_p[F]$
Value	0.08	2000	10	0.01	4.2930	0.3302

Table 5.2: Model parameters for the supercapacitor

A complete charge-discharge cycle is presented in figure 5.2. The charging current is set to 300 [A] until the voltage reaches 800 [V], then the charging current is set to 0 [A] for 10 seconds until the supercapacitor is completely discharged by a current of 300 [A].

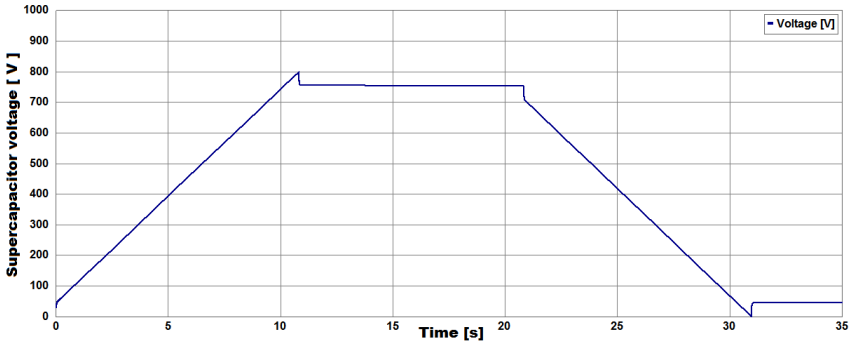

Figure 5.2: Simulation result of a complete charge-discharge cycle of the supercapacitor.

5.1.3 Discussion

The plots presents the typical performance properties in a good way. Figure 5.1 shows the rapid voltage increase which occurs when the battery is fully charged. Figure 5.2 indicated the voltage variations when the charging current is changed. Over the 10 seconds the charging current was set to 0 [A], the self-discharge is negligible.

5.2 Case simulations

Two case simulation are carried out to demonstrate the use of the model. During the first case the load fluctuations are rapid, similar to what is typical during DP-operation. Here the supercapacitor will be used as the energy storage device, due to its ability to serve sudden power demands during fast charging and discharging without any damage. In the second simulation the period of the power fluctuations are longer, and the battery will be used for energy storage. Such operation profiles can be relevant for tugboats and for platform supply vessels during maneuvering and DP-operation. The two effort sources supplies the inverter with 400 [V] on the positive side and -400 [V] on the negative side for both case simulations. $P_{G,lim}$ is chosen to be 150 [kW].

5.2.1 Case 1 - DP-operation with supercapacitor

In case 1 the reference torque follows a sinusoidal curve with a period of 5 seconds, the amplitude is set to 550 [Nm] and the average value is 900 [Nm].

The resistance *R3* is removed from the supercapacitor model (chapter 4.3) during the case simulation since the task of preventing the supercapacitor from overcharging is carried out by the energy management system.

Figure 5.3 presents the load sharing between the source and the supercapacitor during the fluctuating load demand. The resulting supercapacitor voltage is shown in the middle plot, while the corresponding current is displayed in the lower plot. Positive current is equivalent to charging the supercapacitor.

The two plots in figure 5.4 presents the electromagnetic torque and the propeller speed.

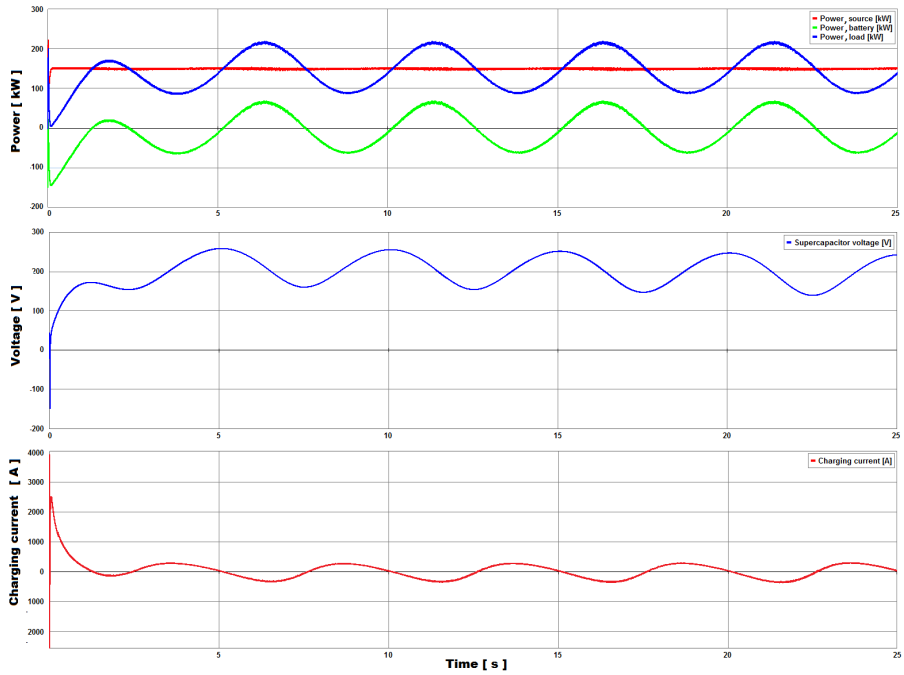

Figure 5.3: Load sharing, supercapacitor voltage and charging current.

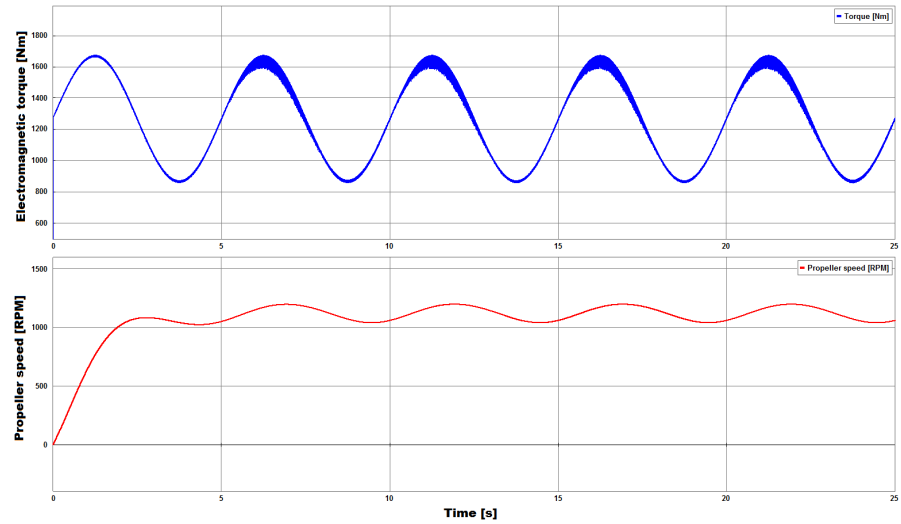

Figure 5.4: Propeller speed and electromagnetic torque

5.2.2 Comments to case 1

The results in figure 5.3 confirms that during low load conditions the current to the supercapacitor is positive and voltage increases as the supercapacitor is charged. During high load conditions on the other hand, current is drawn from the supercapacitor and the voltage decreases as it discharges. As a consequence, the power supplied by the power source remains constant. The load disturbances of the power plant is thereby reduced which facilitates for stable operation of the generator set.

A criteria for the reducing the load fluctuations seen by the diesel engines is that the supercapacitor voltage is kept within its limits.

Rapid variations of the electromagnetic torque produced by the DTC controller can be seen in figure 5.3. The level of variation is significantly reduced by decreasing the simulation time step. As a result, a trade-off between simulation time and level of torque variations was necessary.

5.2.3 Case 2 - Operation with a battery pack

Case 2 simulates the system performance while using the battery for energy storage. The reference torque was varied according to table 5.3. The lower and upper SOC-limitation was set to 40 %and 100 % respectively.

Time [s]	$\mathbf{T_{ref}}$ [Nm]
0 - 30	1300
30 - 60	1500
60 - 100	1000
100 - 140	1550
140 - 170	1050
170 - 200	1350
200 - 220	750
220 - 270	1600
270 - 300	1000

Table 5.3: Reference torque

The load sharing between the source and the battery during varying load demand is presented in the first plot of figure 5.5. The middle plot shows the resulting SOC curve, while the lower plot presents the charging current. Positive current means that the battery is charged.

Figure 5.6 displays the electromagnetic torque of induction motor rotor in the top plot. The corresponding propeller speed can be seen in the lower plot.

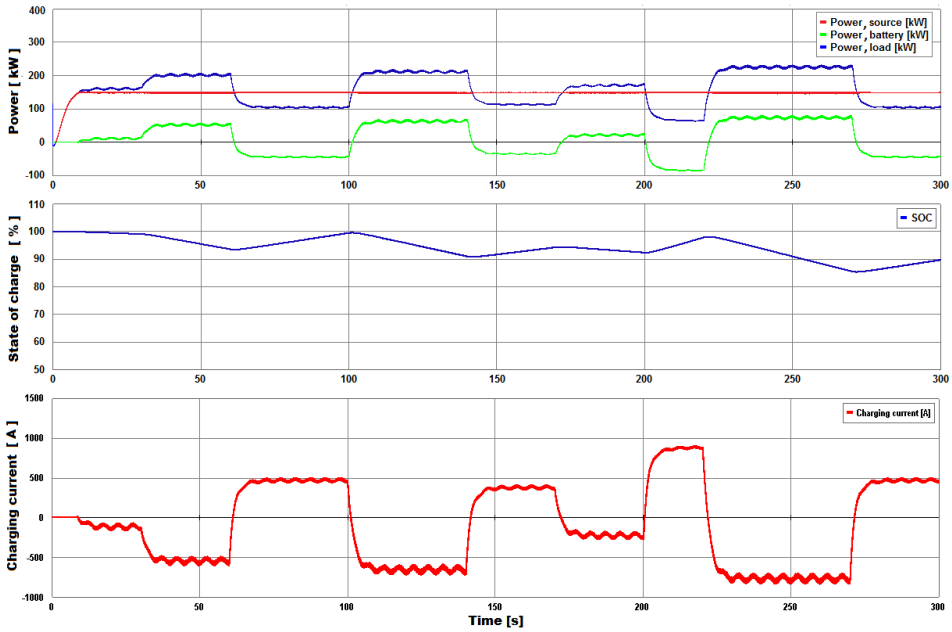

Figure 5.5: Load sharing, SOC and charging current from case simulation 2.

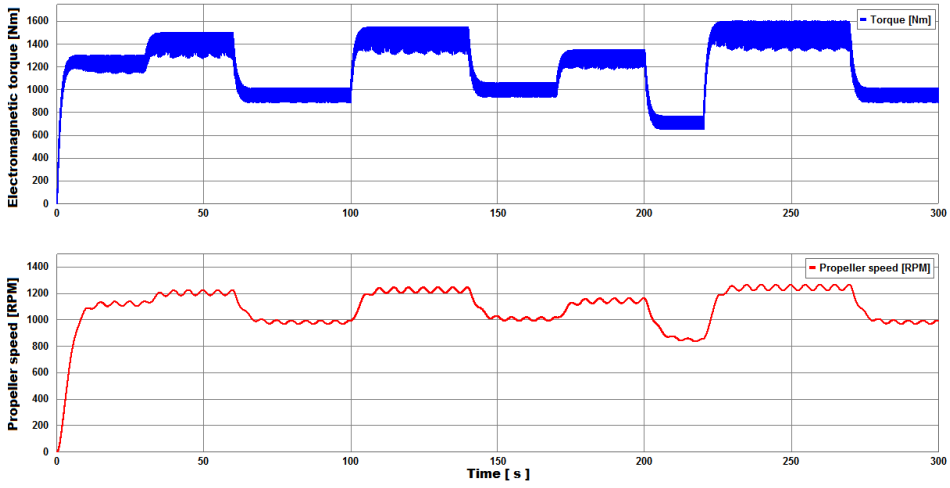

Figure 5.6: Propeller speed and electromechanical torque.

5.2.4 Comments to case 2

In the same way as for case 1, the results from case 2 show that while the load is below the power limitation of the source the battery is charged, the state of charge increases and the current to the battery is positive. While the load is above the power limitation of the source the battery is discharged, the state of charge decreases and the charging current in negative. As a result the load profile seen by the power source stays almost constant. During the first 10 seconds of the simulation, P_{load} is below $P_{G,lim}$, but there still is no power consumed for charging the battery. This is a result of the battery initially being fully charged and the energy management system protecting it from overcharging.

The wave disturbances on the propeller is transmitted to back to the DC-bus and the effect is visible in several plots. Because the battery acts as a energy buffer, the disturbances will influence the operational conditions of the prime mover.

In the same way as for case 1 there exist rapid variations of the electromagnetic torque of the rotor in the induction motor. The level of variations is increased compared to case 1, mainly due to a larger time step in the simulation.

Chapter 6

Conclusions and recommendations

The current development in marine power systems suggest that hybrid technology will be found in an increasing number of applications in the years to come. Continuously improvements in the energy storage technology improves the potential for economical benefits as well as environmental. Stricter environmental regulations and increasing fuel prices will boost the hybridization of the marine industry in the years to come.

The review of the two energy storage concepts in chapter 3 revealed significant differences in performance properties. Of the different battery types, the Li-ion battery is the most promising, because of its low-price and its high energy density. Compared to supercapacitors a typical Li-ion battery has the ability to store 20 - 40 times more energy per unit weight, while the supercapacitor can supply 3-10 times more power. The most beneficial solution is obtained with both devices embedded in the same system and optimizing their interaction based on their different performance properties and limitations.

The bond graph method used for the component modeling proved to be helpful by its ability to indicate the energy flow and causality in electric power systems.

The most important aspect of the produced results is that they confirm the models ability to demonstrate the system behavior as expected. Considering its limitations the model depicts the basic principles of a hybrid marine power plant. The peak shaving effect from the power source point of view is can easily be identified. On the other hand the models accuracy can not be verified without comparing the results with test measurements. The model parameters used for the energy storage components has great influence on the systems behavior. Their chosen values proved to generate the performance results one should expect.

6.1 Recommendations for further work

Hybrid power plants are complex systems and encounters multiple engineering disciplines. Some of the most obvious expansions and features which should be pursued are listed below.

- Development and implementation of component models of generators and diesel engines. Differences in fuel consumption and emissions with and without energy storage can then be estimated.
- Development of tools for temperature monitoring and life-time estimation of the energy storage devices.
- Implementation of sufficient control strategies for power control and system optimizing for fuel efficiency and emissions.
- Verification of the complete model should be carried out, through testing and full-scale measurements.
- Modeling of more realistic environmental loads for different scenarios.

Bibliography

[1] Alf Kåre Ådnanes. *Marine Electrical Installations And Diesel Electric Propulsion*. ABB Marine, 2003.

[2] *Diesel-electric Propulsion Plants, A brief guideline how to engineer a diesel-electric propulsion system* . MAN.

[3] Cummins Inc. *Meeting the Next Challenge, IMO Tier II and III*. 5 - 2011.

[4] DNV Research and Innovation. *Fuel Cells for Ships*. Position Paper 13-2012.

[5] Jack Erjavec. *Hybrid, Electric and Fuel-Cell Vehicles* . 2nd Edition, 2013.

[6] Siemens Innovation News. *First Car Ferry Powered by Electric Drive System*. 2013.

[7] Rakopoulos, Constantine D., Giakoumis, Evangelos G. *Diesel Engine Transient Operation*. Springer-Verlag London Limited, 2009.

[8] Jan F. Hansen, John O. Lindtjørn and Klaus Vanska. *Onboard DC-Grid for enhanced DP operation in ships*. ABB, Dynamic Positioning Conference 2011.

[9] Ru-Shi Liu, Lei Zhang, Xueliang Sun, Hansan Lui and Jiujun Zhang. *Electrochemical Technologies for Energy Storage and Conversion*.Wiley-VCH, Volume 1, 2012.

[10] R. Kötz and M. Carlen. *Principles and applications of electrochemical capacitors*. Electrochimica Acta 45(15-16): 2483-2498, 2000.

[11] Technical Marketing Staff of Gates Energy Products, Inc. *Rechargeable batteries, Applications Handbook*, Elsevier, 1998.

[12] Mukund R. Patel. Shipboard electrical Power System. CRC Press, 2012.

[13] Stanley Atcitty. *Electrochemical Capacitor Characteization for Electric Utility Application*. Virginia Polytechnic Institute and State University, 2006.

[14] Olover Trembley, Louis-A. Desaint, Abdel-Illah Dekkiche. *A Generic Battery Model for the Dynamic Simulation of Hybrid Electric Vehicles*.Ecole de Technologie Supericure, Electric Engineering Department, 2007.

[15] C. M. Shepherd. *Design of Primary and Secondary Cells - Part 2. An equation describing battery discharge*. 1965.

[16] C. Fărcaş, D. Petreuş, I. Ciocan and N. Palaghiţă. *Modeling and Simulation of Supercapacitors*. 2009.

[17] Data sheet for supercapacitor from EPCOS. Part. No.: B48621-S0203-Q288.

[18] Patrik Johansson and Björn Andersson, *Comparison of Simulation Programs for Supercapacitor Modelling. Model Creation and Verification*, Chalmers University of Technology,2008.

[19] Monzer Al Sakka, Hamid Gualous, Noshin Omar and Joeri Van Mierlo, *Batteries and Supercapacitors for Electric Vehicles*. 2012.

[20] Eilif Pedersen and Hallvard Engja. *Mathematical Modelling and Simulation of Physical Systems*. Department of Marine technology, Norwegian University of Science and Technology, 2010.

[21] Tom Arne Pedersen. *Bond Graph Modeling of Marine Power Systems*. Doctoral thesis, Department of Marine technology, Norwegian University of Science and Technology, 2009.

[22] Bibhu P. Panigrahi, Dinkar Prasad and Sabyasachi SenGupta *A simple hardware realization of switching table based direct torque control of induction motor"*, 2007.

[23] Giuseppe Buja and Marian P. Kazmierkowski. *Direct torque control methods for voltage source inverter-fed induction motors - A review"*, 2003.

[24] Sergio Junco and Alejandro Donaire. *Bond Graph Modeling and Simulation of Engineering Systems*. Springer Science + Business Media, LLC 2011.

[25] Slobodan N. Vukosavic. *Electrical Machines*. Springer New York, 2013.

[26] P. M. Anderson and A. A. Fouad *Power System Control and Stability*. The Iowa State University Press. Ames, Iowa. 1st edition, 1977.

Appendices

Appendix A

Parameter Calculation for the Induction motor

Data provided by the induction motor manufacturer is presented in the table below:

Rated output	200 kW
Line voltage	400 V
Frequency	50 Hz
Poles	4
Rated speed	1486 RPM
Moment of inertia	3.5 kgm^2
Connection	$\Delta/Delta$
Powerfactor (100% loading)	0.86

Table A.1: Data for the induction motor, Type: M3BP 315MLA 4 IMB35/IM2001

To extract the parameters needed in the model, test results from the manufacturers data sheet where used. The parameter calculations are based on the per-phase equivalent circuit diagram of the induction motor suggested by [25].

A.1 No-load test

During the test the rotor is unblocked and allowed to run uncoupled from any mechanical load at rated voltage and frequency. The input current, voltage and power is measured in addition to core losses, winding losses and friction. When the motor is uncoupled from any mechanical load the rotor revolves with no external resistance. The load torque is zero and mechanical losses are negligible in most cases. As a result the relative slip is close to zero and the rotor rotates at almost synchronous speed, n_s. The rotor resistance R_2 becomes so large that the rotor current is negligible and the equivalent circuit diagram reduces to a series con-

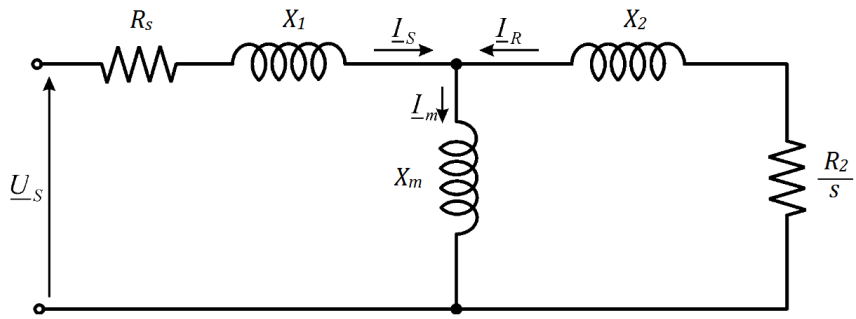

Figure A.1: Equivalent per-phase circuit for an induction motor

nection of the stator resistance R_s, the stator reactance X_s and the magnetizing reactance X_m [25]. The equivalent no-load circuit is presented in figure A.2.

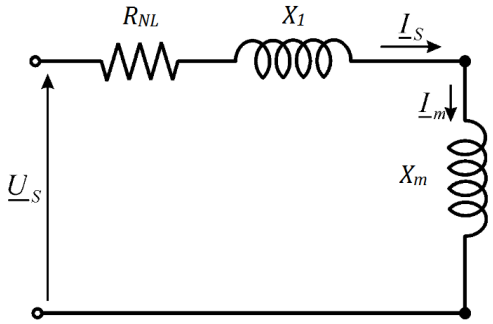

Figure A.2: Equivalent per-phase circuit of the induction motor during No-load test

Power input, P_{NL}	3.14 kW
Line, voltage, V_l	399.8 V
Frequency, f	50 Hz
Line current, I_l	111.8 A
Power factor, p.f	0.04
Speed, n	1500 RPM

Table A.2: Results from No-load test

The expressions for the no-load impedance, resistance and reactance depends on the type of connection configuration. For a delta connected induction motor the

expressions are given by:

No-load impedance:

$$Z_{NL} = \frac{V_l\sqrt{3}}{I_l} = \frac{399.8 \cdot \sqrt{3}}{111.8} = 6.194[\Omega] \tag{A.1.1}$$

No-load resistance:

$$R_{NL} = \frac{P_{NL}}{I_l^2} = \frac{3.14 * 10^3}{111.8^2} = 0.2512[\Omega] \tag{A.1.2}$$

No-load reactance:

$$X_{NL} = X_1 + X_M = \sqrt{Z_{NL}^2 - R_{NL}^2} = \sqrt{6.194^2 - 0.2512^2} = 6.189[\Omega] \tag{A.1.3}$$

A.2 Blocked rotor test

In the blocked rotor test, both the rotor and the stator currents has the line frequency. The rotor is blocked, resulting an a slip equal to unity. The equivalent per-phase circuit reduces to a series connection consisting of the stator resistance R_s, the stator reactance X_s, the rotor reactance X_2 and the rotor resistance R_2 [25].

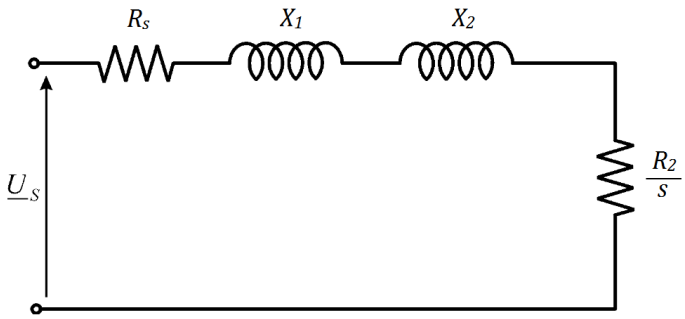

Figure A.3: Equivalent per-phase circuit of the induction motor during the blocked rotor test.

Power input, P_{BL}	13.5 kW
Line, voltage, V_l	71.9 V
Frequency, f	50 Hz
Line current, I_{BL}	351.6 A
Power factor, $cos(\phi)$	0.31
Speed, n	0 RPM

Table A.3: Results from blocked rotor test

The blocked rotor resistance is found by:

$$R_{BL} = \frac{P_{BL}}{I_l^2} = 0.1092[\Omega] \tag{A.2.1}$$

Assuming that R_1 is half of R_{BL} gives:

$$R_1 = 0.5460[\Omega] \tag{A.2.2}$$

The rotor resistance if found by subtracting the stator resistance from the total resistance measured during the blocked rotor test.

$$R_2 = R_{BL} - R_1 = 0.1092 - 0.05460 = 0.05460[\Omega] \tag{A.2.3}$$

$$Z_{BL} = \frac{V_l\sqrt{3}}{I_l} = \frac{71.9 \cdot \sqrt{3}}{351.6} = 0.3541[\Omega] \tag{A.2.4}$$

$$X_{BL} = \sqrt{Z_{BL}^2 - R_{BL}^2} = \sqrt{0.3541^2 - 0.1092^2} = 0.3369[\Omega] \tag{A.2.5}$$

To find the blocked rotor reactance we assume that the ratio between rotor and stator reactance is equal to 1.35, which is a reasonable value for this type of induction motor [21].

$$X_{BL} = X_1 + X_2 = X_1 + \frac{1}{1.35}X_1 \tag{A.2.6}$$

Which gives

$$X_1 = \frac{1.35}{2.35} \cdot X_{BL} = 0.1935[\Omega] \tag{A.2.7}$$

$$X_2 = \frac{1}{1.35} \cdot X_1 = 0.1433[\Omega] \tag{A.2.8}$$

The magnetizing reactance:

$$X_m = X_{NL} - X_1 = 6.189 - 0.1935 = 5.995[\Omega] \tag{A.2.9}$$

All parameters of the equivalent per-phase circuit is presented in table A.4.

Stator resistance	R_1	0.0546 [Ω]
Rotor resistance	R_2	0.0546 [Ω]
Stator reactance	X_1	0.1935 [Ω]
Rotor reactance	X_2	0.1433 [Ω]
Magnetizing reactance	X_m	5.9950 [Ω]

Table A.4: The parameters of the equivalent per-phase circuit for the induction motor

A.3 Calculation of inductance parameters and rotational losses

For a delta-connected induction motor the following relations are valid:

$$V_{rms} = U_l = 400[V] \tag{A.3.1}$$

$$I_{rms} = \frac{I_l}{\sqrt{3}} = \frac{352.1}{\sqrt{3}} = 203.3[A] \tag{A.3.2}$$

$$V_{ref} = \sqrt{2}U_{rms} = \sqrt{2} \cdot 400V = 565.7[V] \tag{A.3.3}$$

$$I_{ref} = \sqrt{2}I_{rms} = \sqrt{2} \cdot 203.3 = 287.5[A] \tag{A.3.4}$$

$$Z_{ref} = \frac{V_{ref}}{I_{ref}} = \frac{565.7}{287.5} = 1.967[\Omega] \tag{A.3.5}$$

$$L_{ref} = \frac{Z_{ref}}{\omega_r} = \frac{565.7}{2\pi \cdot 50} = 0.006263[H] \tag{A.3.6}$$

The per unit values (p.u.) for the inductances can now be calculated by:

$$L_{spu} = \frac{X_s}{Z_{ref}} = \frac{X_1 + X_m}{Z_{ref}} = 3.145 \tag{A.3.7}$$

$$L_{rpu} = \frac{X_r}{Z_{ref}} = \frac{X_2 + X_m}{Z_{ref}} = 3.120 \tag{A.3.8}$$

$$L_{mpu} = \frac{X_m}{Z_{ref}} = 3.406 \tag{A.3.9}$$

The actual inductances are is expressed by:

$$L_s = L_{spu}L_{ref} = 0.01970[H] \tag{A.3.10}$$

$$L_r = L_{rpu}L_{ref} = 0.01954[H] \tag{A.3.11}$$

$$L_m = L_{mpu} L_{ref} = 0.01908[H] \tag{A.3.12}$$

The rotational losses on the mechanical side of the induction motor can be found using the results form the no-load test. Subtracting the stator copper losses from the no-load power will give us the rotational power loss.

$$P_{rloss} = P_{NL} - 3I_s^2 R_1 = 2.457[kW] \tag{A.3.13}$$

The relation between the friction torque and the rotational speed is assumed to be non-linear. The friction torque is expressed by:

$$T_{fric} = C_{fric}(\frac{\omega}{\omega_r})^{0.1} \tag{A.3.14}$$

where the rated angular motor speed, ω_r is found by:

$$\omega_r = \frac{2\pi f}{P} = \frac{2\pi \cdot 50}{2} = 157.08[rad/s] \tag{A.3.15}$$

C_{fric}, represents the friction coefficient, and is determined by:

$$C_{fric} = \frac{P_{rot}}{\omega_r} = 15.6417[Nm] \tag{A.3.16}$$

A.4 Test report of the induction motor

Test Report

Date of issue: 29.1.2012

Serial No.: 3GF10056621

Type: M3BP 315MLA 4 IMB35/IM2001
Product Code: 3GBP312410-ADG
Protection type:
Cert. No.:

Rating:

	V		Hz	kW	r/min	A	cos φ	Duty
3~Motor	400	D	50	200	1486	351	0.86	S1

Insul.cl.F
IP55

Resistance
Line — Ambient: 20,0 °C
U_1 - V_1 0,01020 Ω
U_1 - W_1 0,01021 Ω
V_1 - W_1 0,01020 Ω

Insulation resistance at 57,5 °C
2400 MΩ 1000 V

Overload
Torque 160 % 15s

High-voltage test winding 2400 V 60 s

Test	Torque [Nm]	Line U[V]		f[Hz]	Input I[A]	P1 [kW]	Output P2 [kW]	n[r/min]	cos φ	η [%]
No load test		399,8	D	50	111,8	3,14		1500	0,04	
Locked rotor test		71,9	D	50	351,6	13,5		0	0,31	
Thermal test (100% load)	1285,0	400,1	D	50	352,1	209,3	200,0	1487	0,86	95,5
Partial load points:										
~75% load	964,2	400,1	D	50	272,8	156,7	150,0	1490	0,83	95,7
~50% load	645,3	400,0	D	50	201,1	104,8	100,0	1492	0,75	95,4

Test	Torque [Nm]	Line U[V]		f[Hz]	Input I[A]	P1 [kW]	Output P2 [kW]	n[r/min]	cos φ	η [%]
No load test		399,8	D	50	111,8	3,14		1500	0,04	
Locked rotor test		71,9	D	50	351,6	13,5		0	0,31	
Thermal test (100% load)	1285,0	400,1	D	50	352,1	209,3	200,0	1487	0,86	95,5
Partial load points:										
~75% load	964,2	400,1	D	50	272,8	156,7	150,0	1490	0,83	95,7
~50% load	645,3	400,0	D	50	201,1	104,8	100,0	1492	0,75	95,4
~25% load	322,0	400,1	D	50	142,1	53,6	50,0	1496	0,54	93,3

Temperature rise at rated load.	[°C]	[K]	Method
Stator winding :		73,3	1
Frame :		46,0	2
Bearing D-end :		50,2	2
Ambient Temperature :	25,0		2

Measurement method
1 Resistance
2 Thermometer
3 Thermocouples

Manufactured and tested in accordance with rules of IEC 60034-1 and IEC 60034-2-1.
PLL determined from residual loss.

On behalf of customer

On behalf of manufacturer Date of test 18.1.2011

Tested by ABB Oy, Motors and Generators, Vaasa, Finland

Telephone +358 10 2211
Telefax +358 10 22 47372

Computer print-out valid without signature.

ABB, Motors and Generators
www abb.com/motors&generators

Appendix B

Source code from 20-Sim

This appendix presents the code from 20-sim for the main components.

B.1 Mse, battery

```
parameters
   real K= 0.03;          //Polarization constant
   real A= 0.9;           //Amplitude of axponential zone
   real B= 0.005;         //Inverse of exponential zone time constant
   real global Q= 286200; //Battery capacity, [As]
   real E= 96;            //Constant battery Voltage
variables
   real flow;
equations
//Battery Voltage:
   p.e=(E-(K*(Q/(Q-it))))+(A*exp(-B*it));
   flow = p.f;
```

B.2 SOC-Calculator

```
//SOC CALCULATOR
//***************
parameters
   real global Q;// Battery capacity, [Ah]
equations
   SOC=((Q-charge)/Q)*100;
```

B.3 Torque and flux determination

```
//TORQUE AND FLUX ESTIMATION
//**************************
parameters
//Stator resistance:
   real Rs= 0.0546;
variables
   real Vab,Vbc,V_as,V_bs,I_as,I_bs,psi_as,psi_bs,ratio;
equations
//Line-to-line voltages
   Vab=Va-Vb;
   Vbc=Vb-Vc;

//Stator voltages in alfa-beta-frame:
   V_as=(sqrt(2.0/3.0)*Vab) + (1.0/(sqrt(6.0)))*Vbc;
   V_bs=(1/sqrt(2))*Vbc;

//Stator currents in alfa-beta-frame:
   I_as=(sqrt(2.0/3.0))*(Ia-(Ib/2.0)-(Ic/2.0));
   I_bs=(1/sqrt(2))*(Ib-Ic);

//Stator flux in alfa-beta-frame:
   psi_as=int(V_as-Rs*I_as);
   psi_bs=int(V_bs-Rs*I_bs);

//The electromagnetic torque:
   Te=2*(psi_as*I_bs-psi_bs*I_as);

//The magnitude of the stator flux:
   Psi=sqrt((psi_as^2)+(psi_bs^2));

//Sector determination:
   ratio=abs(psi_bs/(psi_as+1e-10));

   if ratio < (1/sqrt(3)) then
      A1=0;
   else
      A1=1;
   end;

   if psi_as > 0 then
      A2=1;
   else
      A2=0;
   end;

   if psi_bs > 0 then
      A3=1;
   else
      A3=0;
   end;
```

B.4 Switching table

```
//SWITCHING TABLE:
//*****************
variables
   integer d_psi,d_T; // Flux and torque decision variable
equations
   if Psi_error > 0 then
      d_psi=1;    //Increase stator flux
   else
      d_psi=0;    //Decrease stator flux
   end;

   if T_error == 0 then
      d_T=0;               //Maintain torque
   else if T_error <0 then
      d_T=-1;              //Decrease torque
   else
      d_T=1;               //Increase torque
   end;
   end;

   if Sector == 1 and d_psi==1 and d_T==1 then
      S1=1;S2=1;S3=0;
   else if  Sector == 1 and d_psi==1 and d_T==0 then
      S1=1;S2=1;S3=1;
   else if  Sector == 1 and d_psi==1 and d_T==-1 then
      S1=1;S2=0;S3=1;
   else if  Sector == 1 and d_psi==0 and d_T==1 then
      S1=0;S2=1;S3=0;
   else if  Sector == 1 and d_psi==0 and d_T==0 then
      S1=0;S2=0;S3=0;
   else if  Sector == 1 and d_psi==0 and d_T==-1 then
      S1=0;S2=0;S3=1;

   else if  Sector == 2 and d_psi==1 and d_T==1 then
      S1=0;S2=1;S3=0;
   else if  Sector == 2 and d_psi==1 and d_T==0 then
      S1=0;S2=0;S3=0;
   else if  Sector == 2 and d_psi==1 and d_T==-1 then
      S1=1;S2=0;S3=0;
   else if  Sector == 2 and d_psi==0 and d_T==1 then
      S1=0;S2=1;S3=1;
   else if  Sector == 2 and d_psi==0 and d_T==0 then
      S1=1;S2=1;S3=1;
   else if  Sector == 2 and d_psi==0 and d_T==-1 then
      S1=1;S2=0;S3=1;
```

```
else if  Sector == 3 and d_psi==1 and d_T==1 then
      S1=0; S2=1;S3=1;
else if  Sector == 3 and d_psi==1 and d_T==0 then
      S1=1;S2=1;S3=1;
else if  Sector == 3 and d_psi==1 and d_T==-1 then
      S1=1;S2=1;S3=0;
else if  Sector == 3 and d_psi==0 and d_T==1 then
      S1=0;S2=0;S3=1;
else if  Sector == 3 and d_psi==0 and d_T==0 then
      S1=0;S2=0;S3=0;
else if  Sector == 3 and d_psi==0 and d_T==-1 then
      S1=1;S2=0;S3=0;

else if  Sector == 4 and d_psi==1 and d_T==1 then
      S1=0;S2=0;S3=1;
else if  Sector == 4 and d_psi==1 and d_T==0 then
      S1=0;S2=0;S3=0;
else if  Sector == 4 and d_psi==1 and d_T==-1 then
      S1=0;S2=1;S3=0;
else if  Sector == 4 and d_psi==0 and d_T==1 then
      S1=1;S2=0;S3=1;
else if  Sector == 4 and d_psi==0 and d_T==0 then
      S1=1;S2=1;S3=1;
else if  Sector == 4 and d_psi==0 and d_T==-1 then
      S1=1;S2=1;S3=0;

else if  Sector == 5 and d_psi==1 and d_T==1 then
      S1=1;S2=0;S3=1;
else if  Sector == 5 and d_psi==1 and d_T==0 then
      S1=1;S2=1;S3=1;
else if  Sector == 5 and d_psi==1 and d_T==-1 then
      S1=0;S2=1;S3=1;
else if  Sector == 5 and d_psi==0 and d_T==1 then
      S1=1;S2=0;S3=0;
else if  Sector == 5 and d_psi==0 and d_T==0 then
      S1=0;S2=0;S3=0;
else if  Sector == 5 and d_psi==0 and d_T==-1 then
      S1=0;S2=1;S3=0;

else if  Sector == 6 and d_psi==1 and d_T==1 then
      S1=1;S2=0;S3=0;
else if  Sector == 6 and d_psi==1 and d_T==0 then
      S1=0;S2=0;S3=0;
else if  Sector == 6 and d_psi==1 and d_T==-1 then
      S1=0;S2=0;S3=1;
else if  Sector == 6 and d_psi==0 and d_T==1 then
      S1=1;S2=1;S3=0;
else if  Sector == 6 and d_psi==0 and d_T==0 then
      S1=1;S2=1;S3=1;
```

```
else if  Sector == 6 and d_psi==0 and d_T==-1 then
      S1=0;S2=1;S3=1;
end;
end;
end;
end;
end;
end;
end;
end;
end;
end;
end;
end;
end;
end;
end;
end;
end;
end;
end;
end;
end;
end;
end;
end;
end;
end;
end;
end;
end;
end;
end;
end;
end;
end;
end;
end;
```

B.5 Sector determination

```
//Sector determination
//*********************
equations
   if A1==0 and A2==0 and A3==0 then
   Sector=4;
   else if A1==1 and A2==0 and A3==0 then
   Sector=5;
   else if A1==0 and A2==1 and A3==0 then
   Sector=1;
   else if A1==1 and A2==1 and A3==0 then
   Sector=6;
   else if A1==0 and A2==0 and A3==1 then
   Sector=4;
   else if A1==1 and A2==0 and A3==1 then
   Sector=3;
   else if A1==0 and A2==1 and A3==1 then
   Sector=1;
   else if A1==1 and A2==1 and A3==1 then
   Sector=2;
   end;
   end;
   end;
   end;
   end;
   end;
   end;
   end;
```

B.6 1s-junction

```
initialequations
   in.f=0;
equations
   //Calculating the junction flow and effort based on signal S1:
   in.f=S1*out.f+(S1-1)*sf.f;
   sf.e=(S1-1)*out.e;
   out.e=S1*in.e;
```

B.7 0s-junction

```
//Switching of the terminal voltage between Udc/2 and -Udc/2
initialequations
   Va.e=0;
equations
//Calculating the junction effort and flow:
   Va.e = S1*in.e +(1-S1)*out.e;
   in.f = S1*Va.f;
   out.f = (1-S1)*Va.f;
```

B.8 Rotor and propeller inertia

```
parameters
   real i = 50; // Rotor inertia + Propeller inertia
variables
   real RPM;
equations
    state = int(p.e);
    p.f = state / i;
    RPM= p.f*(60/(2*pi));
```

B.9 Propeller load

```
//Propeller load
//****************
parameters
   real K=0.1;//Constant
   real A=0.1;//Amplitude
   real T=5;// Wave period
equations
// The load torque:
   p.e=K*abs(p.f)*p.f*(1+A*(sin(2*pi*time/T)));
```

B.10 TF, induction motor

```
parameters
   real Ppar= 2; //Number of pole pairs
equations
//Calculating output torque and angular velocity:
   p2.e = (Ppar) * p1.e;
   p1.f =  (Ppar) * p2.f;
```

B.11 I, rotor and stator current

```
//Stator and rotor current, d-componenet
//****************************
parameters
   real L_s= 0.01969941;  // Stator inductance
   real L_r= 0.019494036; // Rotor inductance
   real L_m= 0.019083289; // Mutual inductance
variables
   real hidden nevner;
   real hidden Y_ds, Y_dr, i_ds, i_dr;
equations
   nevner   = L_s*L_r - L_m^2;
//Flux linkages:
   Y_ds =int(p.e);
   Y_dr =int(P.e);

//Stator and rotor current:
   i_ds  = (Y_ds*L_r - Y_dr*L_m)/nevner;
   i_dr  = (Y_dr*L_s - Y_ds*L_m)/nevner;

//Flow variables
   p.f = i_ds;
   P.f = i_dr;

//Output signal variable
   psi_ds   = Y_ds;
```

B.12 Rotational losses

```
//Rotatinal loss
//**************
parameters
   real C_fric = 15.6417;// Friction coefficient
   real N = 1500; // Rated speed of the induction motor, [RPM]
variables
   real w_ref;
equations
// Rated angular speed, [rad/s]
   w_ref=(N*2*pi)/60;
   p.e = C_fric *((p.f+0.001)/w_ref)^0.1;
```